

THE EFFECT OF TARGET ORIENTATION ON THE MEAN FIRST PASSAGE TIME OF A BROWNIAN PARTICLE TO A SMALL ELLIPTICAL ABSORBER.

SANCHITA CHAKRABORTY*, THEODORE KOLOKOLNIKOV†, AND ALAN E. LINDSAY‡

Abstract. We develop a high order asymptotic expansion for the mean first passage time (MFPT) of the capture of Brownian particles by a small elliptical trap in a bounded two dimensional region. This new result describes the effect that trap orientation plays on the capture rate and extends existing results that give information only on the role of trap position on the capture rate. Our results are validated against numerical simulations which confirm the accuracy of the asymptotic approximation. In the case of the unit disk domain, we identify a bifurcation such that the high order correction to the global MFPT (GMFPT) is minimized when the trap is orientated in the radial direction for traps centered at $0 < r < r_c := \sqrt{2} - \sqrt{2}$. When centered at position $r_c < r < 1$, the GMFPT correction is minimized by orientating the trap in the angular direction. In the scenario of a general two-dimensional geometry, we identify the orientation that minimizes the GMFPT in terms of the regular part of the Neumann Green's function. This theory is demonstrated on several regular domains such as disks, ellipses and rectangles.

Key words. Singular perturbations, Brownian motion, Narrow escape problem.

1. Introduction. We consider the problem of describing the mean first passage time (MFPT) of two dimensional Brownian motion in a bounded region to a small elliptical absorbing trap. The diffusive transport of molecules and individual agents from a source to a mobile or fixed target is a problem occurring in a variety of physical, biological and social systems [16, 34, 39]. Ecological examples include the time required for an animal to find a mate or shelter [11, 25, 40]. At the cellular scale, diffusion transports key cargoes within the cell [8, 12, 13, 15, 26], including fibroblasts to initiate wound healing [1], antigens for detection by T-cell receptors [35, 36], and material to and from the nucleus [28, 42]. The scope of the target search problem has also been expanded to include features such as stochastic switching of target states, resetting [6], extreme statistics, and homogenization [38]. For an extensive review, we point the reader to the recent survey [14].

The MFPT $u(\mathbf{x})$ describing the expected time to capture a diffusing particle initially at $\mathbf{x} \in \Omega \setminus \Omega_\varepsilon$ solves the Poisson equation [5, 16]

$$(1.1a) \quad D\Delta u + 1 = 0, \quad \mathbf{x} \in \Omega \setminus \Omega_\varepsilon;$$

$$(1.1b) \quad D\nabla u \cdot \hat{\mathbf{n}} = 0, \quad \mathbf{x} \in \partial\Omega;$$

$$(1.1c) \quad u = 0, \quad \mathbf{x} \in \partial\Omega_\varepsilon.$$

The boundary conditions (1.1b) prescribe that the outer boundary $\partial\Omega$ is reflecting and equation (1.1c) specifies that the trap Ω_ε is absorbing. The aim of this paper is to construct a solution to (1.1) in the limit as $\varepsilon \rightarrow 0$ in the presence of an elliptical trap defined as

$$(1.2) \quad \Omega_\varepsilon = \boldsymbol{\xi} + \varepsilon e^{i\phi} \mathcal{A}, \quad \mathcal{A} = \left\{ (y_1, y_2) \in \mathbb{R}^2 \mid \frac{y_1^2}{a^2} + \frac{y_2^2}{b^2} < 1 \right\}.$$

Here εa and εb are the semi-major and semi-minor axes respectively and ϕ is the angle of orientation with respect to the horizontal axis (see Fig. 1). The term $e^{i\phi}$ corresponds to rotation by angle ϕ in the counter clockwise direction. An important quantity, called the global MFPT (GMFPT), describes the overall capture rate based on a uniform distribution of start locations, and is defined as

$$(1.3) \quad \tau = \frac{1}{|\Omega \setminus \Omega_\varepsilon|} \int_{\Omega \setminus \Omega_\varepsilon} u(\mathbf{x}) d\mathbf{x}.$$

Before outlining the rationale for this work and relationship to previous studies, we state our main result:

*Department of Applied and Computational Mathematics and Statistics, University of Notre Dame, Notre Dame, IN, 46656, USA. schakra2@nd.edu

†Department of Mathematics, Dalhousie University, Halifax, Nova Scotia, Canada, B3H 3J5. tkolokol@gmail.com

‡Department of Applied and Computational Mathematics and Statistics, University of Notre Dame, Notre Dame, IN, 46656, USA. a.lindsay@nd.edu

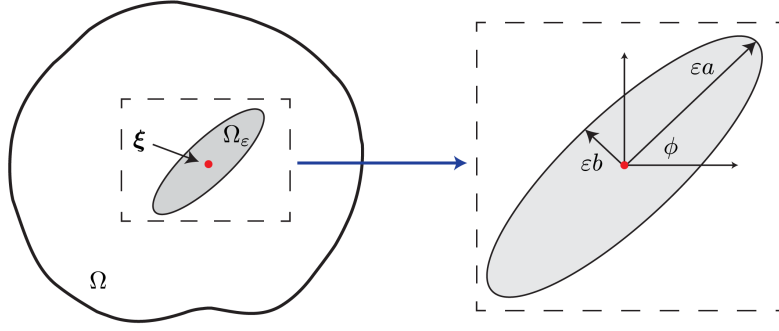


FIG. 1. Schematic of the configuration of the domain Ω with a single trap Ω_ε as defined in (1.3). The trap is centered at $\xi \in \Omega$ and has semi-major and semi-minor axes εa and εb respectively. The semi-major axis of the trap is orientated at angle ϕ with respect to the horizontal axis.

Principal Result: Consider equation (1.1) with a single elliptical trap centered at $\xi \in \Omega$ with semi-major and semi-minor axes εa and εb respectively ($a > b$) and the semi-major axis having elevation ϕ from the horizontal. In the limit as $\varepsilon \rightarrow 0^+$, a two term expansion of the solution to (1.1) and the GMFPT (1.3) is of form

$$(1.4a) \quad u(\mathbf{x}) = \frac{1}{D} [u_0(\mathbf{x}) + \varepsilon^2 u_2(\mathbf{x}) + \mathcal{O}(\varepsilon^4)]; \quad \tau = \frac{1}{D} [\tau_0 + \varepsilon^2 \tau_2 + \mathcal{O}(\varepsilon^4)].$$

The terms in the above expansions are given explicitly as

$$(1.4b) \quad u_0(\mathbf{x}) = -|\Omega| \left[G(\mathbf{x}; \xi) - R(\xi; \xi) \right] + \frac{|\Omega|}{2\pi\nu};$$

$$(1.4c) \quad u_2(\mathbf{x}) = |\Omega| \left[\frac{1}{2} \text{Trace}(\mathcal{Q} \nabla_\xi^2 G(\mathbf{x}; \xi)) - 2\pi \nabla_\xi R(\xi; \xi) \cdot \mathcal{M} \nabla_\xi G(\mathbf{x}; \xi) \right] + \chi_2.$$

The logarithmic gauge function is $\nu(\varepsilon) = -1/\log(\varepsilon d_c)$ where d_c is the logarithmic capacitance which reflects the shape of the trap and is determined by (B.81). For an elliptical trap, $d_c = \frac{1}{2}(a + b)$. The constant χ_2 is given by

$$(1.4d) \quad \chi_2 = -|\Omega| \left(\text{Trace}(\mathcal{Q} \nabla_\xi^2 R(\xi; \xi)) - 2\pi \nabla_\xi R(\xi; \xi) \cdot \mathcal{M} \nabla_\xi R(\xi; \xi) \right) + \frac{a^2 + b^2}{8}.$$

Here \mathcal{Q} and \mathcal{M} are the quadrupole and moment polarization matrices and solve associated electrified disk problems (B.81) and (B.84), respectively. For the case of an elliptical trap, they are given explicitly by

$$(1.4e) \quad \mathcal{Q} = -\frac{a^2 - b^2}{4} \begin{bmatrix} \cos 2\phi & \sin 2\phi \\ \sin 2\phi & -\cos 2\phi \end{bmatrix}, \quad \mathcal{M} = -\frac{(a+b)^2}{4} \mathcal{I} + \mathcal{Q}.$$

The terms of the GMFPT (1.4a) are given by

$$(1.4f) \quad \tau_0 = \frac{|\Omega|}{2\pi} \left[\frac{1}{\nu} + 2\pi R(\xi; \xi) \right], \quad \nu(\varepsilon) = \frac{-1}{\log(\varepsilon d_c)};$$

$$(1.4g) \quad \tau_2 = \left[\frac{\pi ab}{|\Omega|} \tau_0 + \frac{a^2 + b^2}{8} + \chi_2 \right].$$

In the above result $G(\mathbf{x}; \xi)$ and $R(\mathbf{x}; \xi)$ are the Neumann Green's function and its regular part respectively, defined as the unique solution of

$$(1.5a) \quad \Delta G = \frac{1}{|\Omega|} - \delta(\mathbf{x} - \xi), \quad \mathbf{x} \in \Omega; \quad \nabla G \cdot \hat{\mathbf{n}} = 0, \quad \mathbf{x} \in \partial\Omega;$$

$$(1.5b) \quad \int_\Omega G(\mathbf{x}; \xi) d\mathbf{x} = 0; \quad G(\mathbf{x}; \xi) = -\frac{1}{2\pi} \log |\mathbf{x} - \xi| + R(\mathbf{x}; \xi).$$

Before giving a detailed outline of the steps leading to the principal result, we review some recent work on related problems and motivations for this study. Over the past several decades there has been extensive research in the asymptotic analysis of the two-dimensional Poisson problem (1.2) in the presence of small inhomogeneities [7, 17–19, 22, 25, 41] which serves as a canonical problem in the trafficking and delivery of small signaling molecules and cargoes [5]. More generally, there has been significant recent interest in the study of elliptic problems in punctured domains [9, 21, 24, 31–33].

Elliptical traps are of particular interest in cellular signaling problems due to the frequent observation of non-circularity in the cell itself [20] or other key organelles, such as the nucleus [27, 42]. An oval or elliptical geometry accurately captures the aberrations to radial symmetry observed in these domains and hence it is natural to investigate how the capture rate of Brownian particles is modulated by non-circularity. This is one element in a broader mathematical effort to understand the contribution of geometry in cellular signaling [3, 4, 20, 29, 37].

The leading order behavior of the GMFPT (1.4f) as $\varepsilon \rightarrow 0$ (see [25]) captures the effects of trap size and position. However, there is no information on how the orientation of the trap influences the solution. A correction to the leading order behavior (1.4b) was derived in [30] that captures the effect of orientation,

$$(1.6) \quad \tau = \frac{1}{D} [\tau_0 - \varepsilon |\Omega| (\mathbf{d} \cdot \nabla_{\boldsymbol{\xi}} R(\boldsymbol{\xi}; \boldsymbol{\xi})) + \mathcal{O}(\varepsilon^2)].$$

In the result (1.6), the vector \mathbf{d} , is related to the *dipole moment* of the trap and is defined by associated problems that incorporate the shape and orientation of the trap. The contribution to the MFPT from the location of the trap in Ω is captured by the quantity $\nabla_{\boldsymbol{\xi}} R(\boldsymbol{\xi}; \boldsymbol{\xi})$ where the subscript reflects differentiation with respect to the source location.

For application of (1.6) to the case of an elliptical trap, which has two lines of symmetry, we find (see Appendix B.1) that the dipole term vanishes ($\mathbf{d}=\mathbf{0}$), thus (1.6) no longer describes the effect of orientation on the MFPT. Our refined result (1.4) describes the higher order contribution to the MFPT due to the trap orientation. In particular, we can identify optimizing configurations by writing the GMFPT as

$$(1.7) \quad \tau = \frac{\tau_0}{D} + \frac{\varepsilon^2}{D} \left[\frac{\pi ab}{|\Omega|} \tau_0 + \frac{a^2 + b^2}{4} - \pi |\Omega| \frac{(a+b)^2}{2} (R_{\xi_1}^2 + R_{\xi_2}^2) + |\Omega| \frac{a^2 - b^2}{4} \mathbf{p} \cdot \begin{bmatrix} \cos 2\phi \\ \sin 2\phi \end{bmatrix} \right].$$

The vector \mathbf{p} is found to be

$$(1.8) \quad \mathbf{p} = \begin{bmatrix} R_{\xi_1 \xi_1} - R_{\xi_2 \xi_2} - 2\pi(R_{\xi_1}^2 - R_{\xi_2}^2) \\ 2R_{\xi_1 \xi_2} - 4\pi R_{\xi_1} R_{\xi_2} \end{bmatrix},$$

which gives the direction along which the trap should be orientated to optimize the correction term τ_2 of the GMFPT. We note from (1.4f), that when the trap center $\boldsymbol{\xi}$ is placed at a critical point of $R(\boldsymbol{\xi}; \boldsymbol{\xi})$, so that $\nabla_{\boldsymbol{\xi}} R(\boldsymbol{\xi}; \boldsymbol{\xi}) = [R_{\xi_1}, R_{\xi_2}]^T = [0, 0]^T$, the optimal orientation vector reduces to $\mathbf{p} = [R_{\xi_1 \xi_1} - R_{\xi_2 \xi_2}, 2R_{\xi_1 \xi_2}]^T$.

The outline of the paper is as follows. In Sec. 2 we present a hierarchy of results, beginning with the solution of (1.1) in the reduced case of a circular trap located at the center of a disk (Sec. 2.1). Following this, we derive the solution in the presence of an elliptical trap placed at the center of a disk (Sec. 2.2). Finally, we present the corresponding result for the case of a general domain with an ellipse of arbitrary orientation (Sec. 2.3) which yields the principal result (1.4).

In Sec. 3 we first validate the asymptotic result on the unit disk domain where the regular part $R(\mathbf{x}; \boldsymbol{\xi})$ is known in closed form. In this unit disk case, we identify a bifurcation where for $|\boldsymbol{\xi}| > r_c := \sqrt{2 - \sqrt{2}}$, the GMFPT correction term τ_2 is minimized when the semi-major axis is orientated in the angular direction. Conversely, for $|\boldsymbol{\xi}| < r_c$, the GMFPT correction τ_2 is minimized when the semi-major axis is orientated in the radial direction. For certain regular domains, such as rectangles and ellipses, highly accurate series solutions for (1.5) are available, which allows us to determine \mathbf{p} . For these cases we reveal similar bifurcations of the optimizing orientation depending on the centering point of the ellipse $\boldsymbol{\xi}$ and proximity to $\partial\Omega$. Finally in Sec. 4, we discuss avenues for future research arising from this study.

2. Asymptotic analysis of the mean first passage time to a single elliptical trap. In this section we perform the main asymptotic analysis on the MFPT problem (1.1). To guide the rationale for the higher order expansions, it is useful to first analyze two exactly solvable cases for a circular trap located at the center of a disk and an elliptical trap located at the center of a disk.

2.1. Unit disk with a circular trap at the origin. For a single circular trap at the origin, the MFPT (1.1) reduces to the ODE

$$(2.9a) \quad u_{rr} + \frac{1}{r}u_r = -\frac{1}{D}, \quad \varepsilon < r < 1; \quad u(\varepsilon) = u'(1) = 0,$$

where $r = |\mathbf{x}|$. The exact solution of (2.9a) is

$$(2.9b) \quad u(r) = \frac{1}{2D} \left[-\frac{r^2}{2} + \log \frac{r}{\varepsilon} + \frac{\varepsilon^2}{2} \right].$$

The corresponding GMFPT

$$(2.9c) \quad \begin{aligned} \tau &= \frac{1}{|\Omega \setminus \Omega_\varepsilon|} \int_{\Omega \setminus \Omega_\varepsilon} u d\mathbf{x} = \frac{2\pi}{\pi(1-\varepsilon^2)} \int_{r=\varepsilon}^1 u(r)r dr = \frac{1}{8D(1-\varepsilon^2)} \left[-3 + 4\varepsilon^2 - \varepsilon^4 - 4\log \varepsilon \right] \\ &= \frac{1}{8D} \left[-3 - 4\log \varepsilon + \varepsilon^2(1 - 4\log \varepsilon) + \mathcal{O}(\varepsilon^4) \right]. \end{aligned}$$

The equation (2.9c) will be a useful case to validate solutions of (1.1) for more general configurations.

2.2. Unit disk with an elliptical trap at the origin. We now solve for the MFPT in the scenario of an elliptical trap at the origin, orientated along the horizontal axis ($\phi = 0$) with semi-major and semi-minor axes εa and εb respectively.

Outer Expansion We expand as

$$(2.10) \quad u(r) = \frac{1}{D} [u_0(r) + \varepsilon^2 u_2(r, \theta) + \dots]$$

where $\Delta u_0 + 1 = 0$ with $u'_0(1) = 0$ and $\Delta u_2 = 0$ with $u'_2(1) = 0$. The general solutions for u_0 and u_2 in polar coordinates $\mathbf{x} = r e^{i\theta}$ are

$$(2.11a) \quad u_0 = \frac{1}{2} \log r - \frac{r^2}{4} + A_1$$

$$(2.11b) \quad u_2 = B_2 \cos 2\theta (r^2 + r^{-2}) + B_1,$$

for constants A_1, B_1, B_2 to be determined. We remark that in (2.11b), the general solution can accommodate a term of form $\sin 2\theta \times \{r^2, r^{-2}\}$ in the case that the trap orientation moves off the perpendicular axis. Moving to a coordinate $\mathbf{x} = \varepsilon \mathbf{y}$, we find that

$$u \sim \frac{1}{2} \log |\mathbf{y}| + \frac{1}{2} \log \varepsilon + A_1 + B_2 \frac{\cos 2\theta}{|\mathbf{y}|^2} + \varepsilon^2 \left[B_1 - \frac{y^2}{4} \right] + \mathcal{O}(\varepsilon^4).$$

Inner Expansion: In the region $\mathbf{x} = \varepsilon \mathbf{y}$, the solution $u(\mathbf{x}) = U(\mathbf{y})$ is expanded as

$$U(\mathbf{y}) = \frac{1}{D} [U_0(\mathbf{y}) + \varepsilon^2 U_2(\mathbf{y}) + \dots].$$

$\mathcal{O}(\varepsilon^0)$: The leading order problem satisfies

$$(2.12a) \quad \Delta_{\mathbf{y}} U_0 = 0, \quad \text{in } \mathbb{R}^2 \setminus \mathcal{A}; \quad U_0 = 0 \quad \text{on } \partial \mathcal{A};$$

$$(2.12b) \quad U_0 = \frac{1}{2} \log |\mathbf{y}| + \frac{1}{2} \log \varepsilon + A_1 + B_2 \frac{\cos 2\theta}{|\mathbf{y}|^2} + \dots, \quad |\mathbf{y}| \rightarrow \infty.$$

where \mathcal{A} is the rescaled ellipse of semi-major and semi-minor axes a and b respectively with orientation $\phi = 0$ with respect to the origin. Using the solution $v_{0c}(\mathbf{y})$ of the electrified disk problem derived in appendix B.1, we calculate that

$$(2.12c) \quad U_0 = \frac{1}{2}v_{0c}(\mathbf{y}) \sim \frac{1}{2} \left[\log |\mathbf{y}| - \log \alpha - \frac{a^2 - b^2 \cos 2\theta}{4 |\mathbf{y}|^2} + \dots \right], \quad |\mathbf{y}| \rightarrow \infty,$$

where $\alpha = (a + b)/2$. Matching (2.12b) with (2.12c) yields that

$$(2.13) \quad A_1 = \frac{1}{2\nu}, \quad B_2 = -\frac{a^2 - b^2}{8}, \quad \nu = \frac{-1}{\log \varepsilon \alpha}.$$

$\mathcal{O}(\varepsilon^2)$: Proceeding to the next order, we have that

$$(2.14a) \quad \Delta_{\mathbf{y}} U_2 = -1, \quad \text{in } \mathbb{R}^2 \setminus \mathcal{A}; \quad U_2 = 0 \quad \text{on } \partial \mathcal{A};$$

$$(2.14b) \quad U_2 = B_1 - \frac{|\mathbf{y}|^2}{4} + \mathcal{O}(1), \quad |\mathbf{y}| \rightarrow \infty.$$

We solve this problem in appendix B.3 by decomposing the solution as $U_2 = -\frac{1}{4}|\mathbf{y}|^2 + U_{2h}$ where $U_{2h}(\mathbf{y})$ solves a homogeneous problem. We find (see (B.91)) that the large argument behavior of (2.14) is

$$(2.15) \quad U_2 \sim -\frac{|\mathbf{y}|^2}{4} + \frac{a^2 + b^2}{8} + \mathcal{O}(|\mathbf{y}|^{-2}), \quad |\mathbf{y}| \rightarrow \infty.$$

Hence from comparison to (2.14b), we determine that

$$B_1 = \frac{a^2 + b^2}{8}.$$

We remark that the term \mathcal{B}_{11} in (B.91) is determined by the Hessian of the leading outer solution U_0 which vanishes in this case due to the trap being centered at the origin. This completes the derivation of the expansion (2.10) and yields the following expression for the MFPT

$$(2.16) \quad u(r, \theta) = \frac{1}{2D} \left[\log r - \frac{r^2}{2} + \frac{1}{\nu} + \frac{\varepsilon^2}{4} \left((a^2 + b^2) - (a^2 - b^2)(r^2 + r^{-2}) \cos 2\theta \right) \right] + \dots$$

as $\varepsilon \rightarrow 0$. We remark that this expression reduces to the exact solution (2.9b) in the scenario $a = b = 1$. Calculating the GMFPT, we must identify local and global contributions by introducing an intermediate scale $\varepsilon \ll \delta \ll 1$.

$$\tau = \frac{1}{|\Omega \setminus \Omega_\varepsilon|} \int_{\Omega \setminus \Omega_\varepsilon} u \, d\mathbf{x} = \frac{1}{\pi(1 - \varepsilon^2 ab)} \left[\underbrace{\int_{|\mathbf{x}| < \delta} u \, d\mathbf{x}}_{I_1} + \underbrace{\int_{\delta < |\mathbf{x}| < 1} u \, d\mathbf{x}}_{I_2} \right].$$

We proceed to calculate both terms I_1 and I_2 to arrive at a final expression independent of δ .

Calculation of I_1 : Rescaling with $\mathbf{x} = \varepsilon \mathbf{y}$, we have that

$$(2.17) \quad I_1 = \varepsilon^2 \int_{\substack{\mathbf{y} \in \mathbb{R}^2 \setminus \mathcal{A} \\ |\mathbf{y}| < \delta/\varepsilon}} U \, d\mathbf{y} = \frac{\varepsilon^2}{D} \int_{|\mathbf{z}|=1}^{\mathbf{z}=1} \underbrace{(U_0)}_{I_{10}} + \varepsilon^2 \underbrace{(U_1)}_{I_{12}} |J| \, d\mathbf{z}.$$

In the above calculation of the integral I_1 , the region exterior to the ellipse has been mapped to the exterior of the disk through the transformation $\mathbf{y} \rightarrow \alpha \mathbf{z} + \beta/\mathbf{z}$ for $\mathbf{z} = r e^{i\theta}$ and Jacobian $|J|$ given by

$$|J| = \begin{vmatrix} \alpha - \frac{\beta}{r^2} \cos 2\theta & -\frac{\beta}{r^2} \sin 2\theta \\ \frac{\beta}{r^2} \sin 2\theta & \alpha - \frac{\beta}{r^2} \cos 2\theta \end{vmatrix} = \alpha^2 - \frac{2\alpha\beta}{r^2} \cos 2\theta + \frac{\beta^2}{r^4}.$$

Using the fact that $U_0(\mathbf{z}) = \frac{1}{2} \log |\mathbf{z}|$, we have that

$$\begin{aligned} I_{10} &\approx \frac{\varepsilon^2}{2} \int_{\theta=0}^{2\pi} \int_{r=1}^{r=\frac{\delta}{\varepsilon\alpha}} \log r \left(\alpha^2 - \frac{2\alpha\beta}{r^2} \cos 2\theta + \frac{\beta^2}{r^4} \right) r dr d\theta = \varepsilon^2 \pi \int_{r=1}^{r=\frac{\delta}{\varepsilon\alpha}} \log r \left(\alpha^2 r + \frac{\beta^2}{r^3} \right) dr \\ (2.18) \quad &\approx \frac{\pi}{4} \left[\varepsilon^2 (\alpha^2 + \beta^2) + 2\delta^2 \log \frac{\delta}{\varepsilon\alpha} - \delta^2 \right]. \end{aligned}$$

The contribution from I_{12} is $\mathcal{O}(\varepsilon^4)$. We now calculate the contribution from the outer solution.

Calculation of I_2 :

$$\begin{aligned} I_2 &= \frac{1}{D} \int_{|\mathbf{x}|>\delta} (u_0 + \varepsilon^2 u_2) d\mathbf{x} \\ &= \frac{1}{2D} \int_{\theta=0}^{2\pi} \int_{r=\delta}^1 \left[\log r - \frac{r^2}{2} + \frac{1}{\nu} + \frac{\varepsilon^2}{4} \left((a^2 + b^2) - (a^2 - b^2)(r^2 + r^{-2}) \cos 2\theta \right) \right] r dr d\theta \\ &= \frac{\pi}{D} \int_{r=\delta}^1 \left[\log r - \frac{r^2}{2} + \frac{1}{\nu} + \frac{\varepsilon^2}{4} (a^2 + b^2) \right] r dr \\ (2.19) \quad &\approx \frac{\pi}{4D} \left[-\frac{3}{2} + \frac{2}{\nu} + \frac{\varepsilon^2}{2} (a^2 + b^2) - 2\delta^2 \log \delta + \delta^2 - \frac{2\delta^2}{\nu} \right] \end{aligned}$$

Combining these two terms, we have that

$$\begin{aligned} \tau &= \frac{1}{\pi D(1 - \varepsilon^2 ab)} \frac{\pi}{8} \left[-3 + \frac{4}{\nu} + \varepsilon^2 (a^2 + b^2) + 2\varepsilon^2 (\alpha^2 + \beta^2) \right] \\ (2.20) \quad &= \frac{1}{8D} \left[-3 + \frac{4}{\nu} + \varepsilon^2 \left(2(a^2 + b^2) - 3ab + \frac{4ab}{\nu} \right) \right] + \mathcal{O}(\varepsilon^4). \end{aligned}$$

As required, this expression is independent of δ and substitution of $a = b = 1$ reduces (2.20) to (2.9c).

2.3. General case for a single trap. We will now determine the solution to the MFPT problem for a single elliptical domain, centered at $\mathbf{x} = \boldsymbol{\xi}$ with semi-major and semi-minor axes $\varepsilon a, \varepsilon b$, respectively and orientation ϕ with respect to the horizontal axis. The explicit form of the trap is given in (1.2).

In an outer region away from the elliptical trap, we expand the solution as

$$u(\mathbf{x}) = \frac{1}{D} [u_0(\mathbf{x}) + \varepsilon u_1(\mathbf{x}) + \varepsilon^2 u_2(\mathbf{x}) + \mathcal{O}(\varepsilon^2)].$$

The outer problems u_j for $j = 0, 1, 2, \dots$ satisfy

$$(2.21a) \quad \Delta u_j + \delta_{1j} = 0, \quad \mathbf{x} \in \Omega \setminus \{\boldsymbol{\xi}\};$$

$$(2.21b) \quad \nabla u_j \cdot \hat{\mathbf{n}} = 0, \quad \mathbf{x} \in \partial\Omega.$$

The local behavior as $\mathbf{x} \rightarrow \boldsymbol{\xi}$ is now established for each problem (2.21) through boundary layer analysis. In the vicinity of the trap, the solution is expanded in variables

$$(2.22) \quad U = \frac{1}{D} [U_0(\mathbf{y}) + \varepsilon U_1(\mathbf{y}) + \varepsilon^2 U_2(\mathbf{y}) + \mathcal{O}(\varepsilon^2)], \quad \mathbf{y} = e^{-i\phi} \frac{\mathbf{x} - \boldsymbol{\xi}}{\varepsilon}.$$

Collecting terms at relevant orders gives a sequence of problems to be solved.

Inner Region $\mathcal{O}(\varepsilon^0)$: The leading order problem for U_0 satisfies

$$(2.23a) \quad \Delta U_0 = 0, \quad \mathbf{y} \in \mathbb{R}^2 \setminus \mathcal{A};$$

$$(2.23b) \quad U_0 = 0, \quad \mathbf{y} \in \partial\mathcal{A}.$$

In terms of the solution v_{0c} of the electrified disk problem obtained in Appendix B.1, we have that

$$(2.24) \quad U_0(\mathbf{y}) = S\nu v_{0c}(\mathbf{y}), \quad \nu = \frac{-1}{\log \varepsilon \alpha}.$$

Here S is a constant to be determined in the matching process. The far field of equation (2.24) supplies the appropriate local behavior for the outer solution. In (B.81), we establish that for an elliptical trap aligned in the horizontal direction ($\phi = 0$), the far field behavior is

$$(2.25) \quad v_{0c}(\mathbf{y}) = \log |\mathbf{y}| - \log \alpha + \frac{\mathbf{y}^T \tilde{\mathcal{Q}} \mathbf{y}}{|\mathbf{y}|^4}, \quad \tilde{\mathcal{Q}} = -\alpha \beta \begin{bmatrix} 1 & 0 \\ 0 & -1 \end{bmatrix} = -\frac{a^2 - b^2}{4} \begin{bmatrix} 1 & 0 \\ 0 & -1 \end{bmatrix}.$$

Hence, in terms of the outer coordinate $\mathbf{y} = \varepsilon^{-1} e^{-i\phi} (\mathbf{x} - \boldsymbol{\xi})$ incorporating rotation by ϕ with respect to the horizontal, and incorporating the far field behavior for $|\mathbf{y}| \rightarrow \infty$, we generate the local behavior as $\mathbf{x} \rightarrow \boldsymbol{\xi}$

$$(2.26) \quad u \sim S\nu \left[\log |\mathbf{x} - \boldsymbol{\xi}| + \frac{1}{\nu} + \varepsilon^2 \frac{(\mathbf{x} - \boldsymbol{\xi})^T \mathcal{Q} (\mathbf{x} - \boldsymbol{\xi})}{|\mathbf{x} - \boldsymbol{\xi}|^4} \right] + \dots.$$

The matrix $\mathcal{Q} = e^{i\phi} \tilde{\mathcal{Q}} e^{-i\phi}$ is calculated as

$$(2.27) \quad \mathcal{Q} = -\frac{a^2 - b^2}{4} \begin{bmatrix} \cos \phi & -\sin \phi \\ \sin \phi & \cos \phi \end{bmatrix} \begin{bmatrix} 1 & 0 \\ 0 & -1 \end{bmatrix} \begin{bmatrix} \cos \phi & \sin \phi \\ -\sin \phi & \cos \phi \end{bmatrix} = -\frac{a^2 - b^2}{4} \begin{bmatrix} \cos 2\phi & \sin 2\phi \\ \sin 2\phi & -\cos 2\phi \end{bmatrix}.$$

This behavior is used to furnish terms in the outer expansion.

Outer Region $\mathcal{O}(\varepsilon^0)$: The problem at leading order is

$$(2.28a) \quad \Delta u_0 + 1 = 0, \quad \mathbf{x} \in \Omega \setminus \{\boldsymbol{\xi}\};$$

$$(2.28b) \quad \nabla u_0 \cdot \hat{\mathbf{n}} = 0, \quad \mathbf{x} \in \partial\Omega;$$

$$(2.28c) \quad u_0 \sim S\nu \log |\mathbf{x} - \boldsymbol{\xi}| + S + \dots, \quad \mathbf{x} \rightarrow \boldsymbol{\xi}.$$

In terms of the Neumann's Green's function (1.5), we have that

$$(2.29) \quad u_0 = -2\pi S\nu G(\mathbf{x}; \boldsymbol{\xi}) + \tau_0.$$

where τ_0 is a constant. The expansion of u_0 as $\mathbf{x} \rightarrow \boldsymbol{\xi}$ gives the local behavior

$$(2.30) \quad u_0 = S\nu [\log |\mathbf{x} - \boldsymbol{\xi}| - 2\pi R(\mathbf{x}; \boldsymbol{\xi})] + \tau_0 \\ \sim S\nu \log |\mathbf{x} - \boldsymbol{\xi}| + \tau_0 - 2\pi S\nu \left[R(\boldsymbol{\xi}; \boldsymbol{\xi}) + \mathbf{a} \cdot (\mathbf{x} - \boldsymbol{\xi}) + (\mathbf{x} - \boldsymbol{\xi})^T \nabla_{\mathbf{x}}^2 R|_{\mathbf{x}=\boldsymbol{\xi}} (\mathbf{x} - \boldsymbol{\xi}) + \mathcal{O}(|\mathbf{x} - \boldsymbol{\xi}|^3) \right],$$

where the coefficient terms for $\mathbf{x} = (x_1, x_2)$ are given by

$$(2.31) \quad \mathbf{a} := \begin{bmatrix} \partial_{x_1} R(\mathbf{x}; \boldsymbol{\xi}) \\ \partial_{x_2} R(\mathbf{x}; \boldsymbol{\xi}) \end{bmatrix}_{\mathbf{x}=\boldsymbol{\xi}}, \quad \nabla_{\mathbf{x}}^2 R|_{\mathbf{x}=\boldsymbol{\xi}} = \frac{1}{2} \begin{bmatrix} \partial_{x_1 x_1} R(\mathbf{x}; \boldsymbol{\xi}) & \partial_{x_1 x_2} R(\mathbf{x}; \boldsymbol{\xi}) \\ \partial_{x_1 x_2} R(\mathbf{x}; \boldsymbol{\xi}) & \partial_{x_2 x_2} R(\mathbf{x}; \boldsymbol{\xi}) \end{bmatrix}_{\mathbf{x}=\boldsymbol{\xi}} = \frac{1}{2} \begin{bmatrix} R_{11} & R_{12} \\ R_{12} & R_{22} \end{bmatrix}.$$

A system of two equations for unknowns (S, τ_0) is found by both matching (2.29) with the local behavior, and integrating (2.28a). This yields that

$$(2.32) \quad S = \frac{|\Omega|}{2\pi\nu}, \quad \tau_0 = \frac{|\Omega|}{2\pi\nu} \left[1 + 2\pi\nu R(\boldsymbol{\xi}; \boldsymbol{\xi}) \right].$$

This result was established in [22]. We now determine the correction to the inner expansion. In the local variable $\mathbf{y} = \varepsilon^{-1} e^{-i\phi} (\mathbf{x} - \boldsymbol{\xi})$, equation (2.30) yields the far field behavior

$$(2.33) \quad U(\mathbf{y}) \sim S\nu [\log |\mathbf{y}| - \log \alpha - 2\pi\varepsilon \mathbf{a} \cdot e^{i\phi} \mathbf{y} - 2\pi\varepsilon^2 \mathbf{y}^T e^{-i\phi} \nabla_{\mathbf{x}}^2 R|_{\mathbf{x}=\boldsymbol{\xi}} e^{i\phi} \mathbf{y} + \dots], \quad |\mathbf{y}| \rightarrow \infty.$$

This reveals the leading order matching behavior for the higher order inner corrections. Specifically, we have that

$$(2.34a) \quad U_1(\mathbf{y}) \sim -2\pi S\nu \mathbf{a} \cdot e^{i\phi} \mathbf{y} + \dots$$

$$(2.34b) \quad U_2(\mathbf{y}) \sim -2\pi S\nu \mathbf{y}^T e^{-i\phi} \nabla_{\mathbf{x}}^2 R|_{\mathbf{x}=\boldsymbol{\xi}} e^{i\phi} \mathbf{y} + \dots$$

as $|\mathbf{y}| \rightarrow \infty$. This behavior is now matched to corresponding inner problems.

Inner Region $\mathcal{O}(\varepsilon^1)$: At this order we must solve the exterior problem

$$(2.35a) \quad \Delta_{\mathbf{y}} U_1 = 0, \quad \mathbf{y} \in \mathbb{R}^2 \setminus \mathcal{A}; \quad U_1 = 0, \quad \mathbf{y} \in \partial\mathcal{A};$$

$$(2.35b) \quad U_1 = -2\pi S\nu \mathbf{a} \cdot e^{i\phi} \mathbf{y} + \dots, \quad |\mathbf{y}| \rightarrow \infty;$$

In appendix B.2, we introduce and solve the vector valued electrified disk problem \mathbf{v}_{1c}

$$(2.36a) \quad \Delta_{\mathbf{y}} \mathbf{v}_{1c} = 0, \quad \mathbf{y} \in \mathbb{R}^2 \setminus \mathcal{A}; \quad \mathbf{v}_{1c} = 0, \quad \mathbf{y} \in \partial\mathcal{A};$$

$$(2.36b) \quad \mathbf{v}_{1c} = \mathbf{y} + \frac{\tilde{\mathcal{M}}\mathbf{y}}{|\mathbf{y}|^2} + \dots \quad |\mathbf{y}| \rightarrow \infty; \quad \tilde{\mathcal{M}} = -\alpha \begin{pmatrix} a & 0 \\ 0 & b \end{pmatrix}.$$

In terms of this solution, we write that

$$(2.37) \quad U_1 = -2\pi S\nu \mathbf{a} \cdot e^{i\phi} \mathbf{v}_{1c}(\mathbf{y}).$$

Applying the far field behavior (2.36b) as $|\mathbf{y}| \rightarrow \infty$, while returning to outer coordinates with variable $\mathbf{y} = \varepsilon^{-1} e^{-i\phi}(\mathbf{x} - \boldsymbol{\xi})$, we generate the local behavior

$$(2.38a) \quad U_1 \sim -\frac{2\pi S\nu}{\varepsilon} \mathbf{a} \cdot \left[(\mathbf{x} - \boldsymbol{\xi}) + \varepsilon^2 \frac{\mathcal{M}(\mathbf{x} - \boldsymbol{\xi})}{|\mathbf{x} - \boldsymbol{\xi}|^2} \right] + \dots, \quad \text{as } \mathbf{x} \rightarrow \boldsymbol{\xi},$$

In the case of an elliptical trap, we calculate explicitly that $\mathcal{M} = e^{i\phi} \tilde{\mathcal{M}} e^{-i\phi}$ has the form

$$\begin{aligned} \mathcal{M} &= -\alpha \begin{bmatrix} \cos \phi & -\sin \phi \\ \sin \phi & \cos \phi \end{bmatrix} \begin{bmatrix} a & 0 \\ 0 & b \end{bmatrix} \begin{bmatrix} \cos \phi & \sin \phi \\ -\sin \phi & \cos \phi \end{bmatrix} \\ &= -\alpha \begin{bmatrix} a \cos^2 \phi + b \sin^2 \phi & (a-b) \sin \phi \cos \phi \\ (a-b) \sin \phi \cos \phi & b \cos^2 \phi + a \sin^2 \phi \end{bmatrix} \\ &= -\alpha^2 \begin{bmatrix} 1 & 0 \\ 0 & 1 \end{bmatrix} - \alpha \beta \begin{bmatrix} \cos 2\phi & \sin 2\phi \\ \sin 2\phi & -\cos 2\phi \end{bmatrix} \\ (2.38b) \quad &= -\alpha^2 \mathcal{I} + \mathcal{Q}; \end{aligned}$$

where \mathcal{Q} is the quadrupole matrix derived in (2.27).

Inner Region $\mathcal{O}(\varepsilon^2)$: At $\mathcal{O}(\varepsilon^2)$ we introduce the scalar valued problem $U_2(\mathbf{y})$ where

$$(2.39a) \quad \Delta_{\mathbf{y}} U_2 = -1, \quad \mathbf{y} \in \mathbb{R}^2 \setminus \mathcal{A}; \quad U_2 = 0, \quad \mathbf{y} \in \partial\mathcal{A};$$

$$(2.39b) \quad U_2 = -2\pi S\nu \mathbf{y}^T e^{-i\phi} \nabla_{\mathbf{x}}^2 R|_{\mathbf{x}=\boldsymbol{\xi}} e^{i\phi} \mathbf{y} + \dots \quad |\mathbf{y}| \rightarrow \infty;$$

To further decompose the far field behavior (2.39b), we write

$$\begin{aligned} \mathcal{H} &= e^{-i\phi} \nabla_{\mathbf{x}}^2 R|_{\mathbf{x}=\boldsymbol{\xi}} e^{i\phi} \\ &= \frac{1}{2} \begin{bmatrix} \cos \phi & \sin \phi \\ -\sin \phi & \cos \phi \end{bmatrix} \begin{bmatrix} R_{11} & R_{12} \\ R_{12} & R_{22} \end{bmatrix} \begin{bmatrix} \cos \phi & -\sin \phi \\ \sin \phi & \cos \phi \end{bmatrix} \\ &= \frac{R_{11} + R_{22}}{4} \begin{bmatrix} 1 & 0 \\ 0 & 1 \end{bmatrix} + \frac{1}{4} \begin{bmatrix} (R_{11} - R_{22}) \cos 2\phi + 2R_{12} \sin 2\phi & 2R_{12} \cos 2\phi - (R_{11} - R_{22}) \sin 2\phi \\ 2R_{12} \cos 2\phi - (R_{11} - R_{22}) \sin 2\phi & -(R_{11} - R_{22}) \cos 2\phi - 2R_{12} \sin 2\phi \end{bmatrix} \\ &= \frac{R_{11} + R_{22}}{4} \begin{bmatrix} 1 & 0 \\ 0 & 1 \end{bmatrix} + \begin{bmatrix} \mathcal{B}_{11} & \mathcal{B}_{12} \\ \mathcal{B}_{12} & -\mathcal{B}_{11} \end{bmatrix}. \end{aligned}$$

Here \mathcal{B} is the matrix satisfying $\text{Trace}(\mathcal{B}) = 0$ with components

$$(2.40a) \quad \mathcal{B}_{11} = \frac{1}{4} \left[(R_{11} - R_{22}) \cos 2\phi + 2R_{12} \sin 2\phi \right],$$

$$(2.40b) \quad \mathcal{B}_{12} = \frac{1}{4} \left[2R_{12} \cos 2\phi - (R_{11} - R_{22}) \sin 2\phi \right].$$

The far field behavior is now in the form

$$(2.41) \quad \mathbf{y}^T \mathcal{H} \mathbf{y} = \left[(R_{11} + R_{22}) \frac{y_1^2 + y_2^2}{4} + \mathcal{B}_{11}(y_1^2 - y_2^2) + 2\mathcal{B}_{12} y_1 y_2 \right].$$

We remark that $\Delta u_0 = \Delta(S\nu \log |\mathbf{x} - \boldsymbol{\xi}| - 2\pi S\nu R(\mathbf{x}; \boldsymbol{\xi}) + \tau_0) = -1$ which implies that

$$(2.42) \quad \Delta R = R_{11} + R_{22} = \frac{1}{|\Omega|}.$$

After applying these reductions, together with $2\pi S\nu = |\Omega|$ from (2.32), we can restate equation (2.39) as

$$(2.43a) \quad \Delta_{\mathbf{y}} U_2 = -1, \quad \mathbf{y} \in \mathbb{R}^2 \setminus \mathcal{A}; \quad U_2 = 0, \quad \mathbf{y} \in \partial \mathcal{A};$$

$$(2.43b) \quad U_2 \sim -\frac{|\mathbf{y}|^2}{4} - 2\pi S\nu \mathbf{y}^T \mathcal{B} \mathbf{y} + \dots, \quad |\mathbf{y}| \rightarrow \infty.$$

In Appendix B.3, we state and solve the canonical problem (2.43) and obtain the refined behavior

$$(2.44a) \quad U_2 \sim -\frac{|\mathbf{y}|^2}{4} - 2\pi S\nu \mathbf{y}^T \mathcal{B} \mathbf{y} + d_{2c} + \mathcal{O}(|\mathbf{y}|^{-2}), \quad \text{as } |\mathbf{y}| \rightarrow \infty,$$

where the constant term is

$$(2.44b) \quad d_{2c} = \frac{\alpha^2 + \beta^2}{4} + 4\pi S\nu \alpha \beta \mathcal{B}_{11}.$$

If we incorporate the value of \mathcal{B}_{11} shown in (2.40a), this term reduces to

$$(2.45) \quad d_{2c} = \frac{\alpha^2 + \beta^2}{4} - \pi S\nu \text{Trace}(\mathcal{Q} \nabla_{\mathbf{x}}^2 R(\boldsymbol{\xi}; \boldsymbol{\xi})),$$

where we have used the identity

$$\text{Trace}(\mathcal{Q} \nabla_{\mathbf{x}}^2 R(\boldsymbol{\xi}; \boldsymbol{\xi})) = \mathcal{Q}_{11}(R_{11} - R_{22}) + 2\mathcal{Q}_{12}R_{12}; \quad \mathcal{Q} = \begin{bmatrix} \mathcal{Q}_{11} & \mathcal{Q}_{12} \\ \mathcal{Q}_{12} & -\mathcal{Q}_{11} \end{bmatrix} = -\alpha\beta \begin{bmatrix} \cos 2\phi & \sin 2\phi \\ \sin 2\phi & -\cos 2\phi \end{bmatrix}.$$

This completes the solution of the inner expansion (2.22) the inner problem up to $\mathcal{O}(\varepsilon^2)$. A combination of equations (2.26), (2.38) and (2.44) yields the local behavior

$$(2.46) \quad \begin{aligned} u &\sim S\nu \log |\mathbf{x} - \boldsymbol{\xi}| + S \\ &+ \varepsilon^2 \left(S\nu \left[\frac{(\mathbf{x} - \boldsymbol{\xi})^T \mathcal{Q} (\mathbf{x} - \boldsymbol{\xi})}{|\mathbf{x} - \boldsymbol{\xi}|^4} - 2\pi \mathbf{a} \cdot \frac{\mathcal{M}(\mathbf{x} - \boldsymbol{\xi})}{|\mathbf{x} - \boldsymbol{\xi}|^2} \right] + d_{2c} \right) \quad \text{as } \mathbf{x} \rightarrow \boldsymbol{\xi}. \end{aligned}$$

We now return to the outer expansion.

Outer region $\mathcal{O}(\varepsilon^1)$: At this order the problem is given by

$$(2.47a) \quad \Delta u_1 = 0, \quad \mathbf{x} \in \Omega \setminus \{\boldsymbol{\xi}\};$$

$$(2.47b) \quad \nabla u_1 \cdot \hat{\mathbf{n}} = 0, \quad \mathbf{x} \in \partial \Omega;$$

$$(2.47c) \quad u_1 \sim 0, \quad \mathbf{x} \rightarrow \boldsymbol{\xi}.$$

The unique solution of (2.47) is $u_1 \equiv 0$.

Outer region $\mathcal{O}(\varepsilon^2)$: At this order we have that

$$(2.48a) \quad \Delta u_2 = 0, \quad \mathbf{x} \in \Omega \setminus \{\boldsymbol{\xi}\};$$

$$(2.48b) \quad \nabla u_2 \cdot \hat{\mathbf{n}} = 0, \quad \mathbf{x} \in \partial\Omega;$$

$$(2.48c) \quad u_2 \sim S\nu \left[\frac{(\mathbf{x} - \boldsymbol{\xi})^T \mathcal{Q}(\mathbf{x} - \boldsymbol{\xi})}{|\mathbf{x} - \boldsymbol{\xi}|^4} - 2\pi \mathbf{a} \cdot \frac{\mathcal{M}(\mathbf{x} - \boldsymbol{\xi})}{|\mathbf{x} - \boldsymbol{\xi}|^2} \right] + d_{2c} + \dots, \quad \mathbf{x} \rightarrow \boldsymbol{\xi}.$$

To express the solution of (2.48) in terms of the Green's function, we first notice by direct calculation that

$$(2.49a) \quad \nabla_{\boldsymbol{\xi}} \log |\mathbf{x} - \boldsymbol{\xi}| = -\frac{\mathbf{x} - \boldsymbol{\xi}}{|\mathbf{x} - \boldsymbol{\xi}|^2},$$

$$(2.49b) \quad -\frac{1}{2} \text{Trace}(\mathcal{Q} \nabla_{\boldsymbol{\xi}}^2 \log |\mathbf{x} - \boldsymbol{\xi}|) = \frac{(\mathbf{x} - \boldsymbol{\xi})^T \mathcal{Q}(\mathbf{x} - \boldsymbol{\xi})}{|\mathbf{x} - \boldsymbol{\xi}|^4}, \quad \mathcal{Q} = \begin{bmatrix} Q_{11} & Q_{12} \\ Q_{12} & -Q_{11} \end{bmatrix}.$$

The solution of (2.48) can then be written as

$$(2.50) \quad u_2(\mathbf{x}) = S\nu \left[\pi \text{Trace}(\mathcal{Q} \nabla_{\boldsymbol{\xi}}^2 G(\mathbf{x}; \boldsymbol{\xi})) - 4\pi^2 \mathbf{a} \cdot \mathcal{M} \nabla_{\boldsymbol{\xi}} G(\mathbf{x}; \boldsymbol{\xi}) \right] + \chi_2,$$

where χ_2 is a constant to be determined. In the formulation (2.50), the derivatives with respect to the source location $\mathbf{y} = (y_1, y_2)$ are

$$\nabla_{\boldsymbol{\xi}} = \begin{bmatrix} \partial_{\xi_1} \\ \partial_{\xi_2} \end{bmatrix}, \quad \nabla_{\boldsymbol{\xi}}^2 = \begin{bmatrix} \partial_{\xi_1 \xi_1}^2 & \partial_{\xi_1 \xi_2}^2 \\ \partial_{\xi_2 \xi_1}^2 & \partial_{\xi_2 \xi_2}^2 \end{bmatrix}.$$

This in particular leads to the identity

$$(2.51) \quad \text{Trace}(\mathcal{Q} \nabla_{\boldsymbol{\xi}}^2 G(\mathbf{x}; \mathbf{y})) = Q_{11}(G_{y_1 y_1} - G_{y_2 y_2}) + 2Q_{12}G_{y_1 y_2}.$$

To complete the matching, we evaluate (2.50) as $\mathbf{x} \rightarrow \boldsymbol{\xi}$. Since $\mathbf{a} = \nabla_{\mathbf{x}} R(\boldsymbol{\xi}; \boldsymbol{\xi}) = \nabla_{\boldsymbol{\xi}} R(\boldsymbol{\xi}; \boldsymbol{\xi})$, we calculate

$$u_2 \sim \chi_2 + S\nu \left[\frac{(\mathbf{x} - \boldsymbol{\xi})^T \mathcal{Q}(\mathbf{x} - \boldsymbol{\xi})}{|\mathbf{x} - \boldsymbol{\xi}|^4} - 2\pi \mathbf{a} \cdot \frac{\mathcal{M}(\mathbf{x} - \boldsymbol{\xi})}{|\mathbf{x} - \boldsymbol{\xi}|^2} + \pi \text{Trace}(\mathcal{Q} \nabla_{\mathbf{y}}^2 R(\boldsymbol{\xi}; \boldsymbol{\xi})) - 4\pi^2 \mathbf{a} \cdot \mathcal{M} \mathbf{a} \right], \quad \mathbf{x} \rightarrow \boldsymbol{\xi}.$$

Matching with (2.48c), we have that

$$\chi_2 = -S\nu \left(\pi \text{Trace}(\mathcal{Q} \nabla_{\mathbf{y}}^2 R(\boldsymbol{\xi}; \boldsymbol{\xi})) - 4\pi^2 \mathbf{a} \cdot \mathcal{M} \mathbf{a} \right) + d_{2c}.$$

In the case particular to the elliptical trap, we apply (2.38b) so that $\mathcal{M} = -\alpha^2 \mathcal{I} + \mathcal{Q}$. In addition, we apply the value of d_{2c} given in (2.45), together with the symmetry relationship $\nabla_{\mathbf{x}}^2 R(\boldsymbol{\xi}; \boldsymbol{\xi}) = \nabla_{\boldsymbol{\xi}}^2 R(\boldsymbol{\xi}; \boldsymbol{\xi})$, and $S\nu = |\Omega|/2\pi$ from (2.32) to further reduce χ_2 to

$$(2.52) \quad \begin{aligned} \chi_2 &= -S\nu \left(2\pi \text{Trace}(\mathcal{Q} \nabla_{\boldsymbol{\xi}}^2 R(\boldsymbol{\xi}; \boldsymbol{\xi})) + 4\pi^2 \alpha^2 |\mathbf{a}|^2 - 4\pi^2 \mathbf{a} \cdot \mathcal{Q} \mathbf{a} \right) + \frac{a^2 + b^2}{8} \\ &= -|\Omega| \left(\text{Trace}(\mathcal{Q} \nabla_{\boldsymbol{\xi}}^2 R(\boldsymbol{\xi}; \boldsymbol{\xi})) + 2\pi \alpha^2 |\mathbf{a}|^2 - 2\pi \mathbf{a} \cdot \mathcal{Q} \mathbf{a} \right) + \frac{a^2 + b^2}{8} \end{aligned}$$

In summary, the solution of (1.1) admits the expansion $u = \frac{1}{D}[u_0 + \varepsilon^2 u_2 + \dots]$ where the terms are

$$(2.53a) \quad u_0(\mathbf{x}; \boldsymbol{\xi}) = -|\Omega| \left[G(\mathbf{x}; \boldsymbol{\xi}) - R(\boldsymbol{\xi}; \boldsymbol{\xi}) \right] + \frac{|\Omega|}{2\pi\nu},$$

$$(2.53b) \quad u_2(\mathbf{x}; \boldsymbol{\xi}) = |\Omega| \left[\frac{1}{2} \text{Trace}(\mathcal{Q} \nabla_{\boldsymbol{\xi}}^2 G(\mathbf{x}; \boldsymbol{\xi})) - 2\pi \mathbf{a} \cdot \mathcal{M} \nabla_{\boldsymbol{\xi}} G(\mathbf{x}; \boldsymbol{\xi}) \right] + \chi_2.$$

where χ_2 is the constant given in (2.52).

2.4. Calculation of the global MFPT. In this section we calculate the GMFPT defined as

$$\tau = \frac{1}{|\Omega \setminus \Omega_\varepsilon|} \int_{\Omega \setminus \Omega_\varepsilon} u \, d\mathbf{x} = \frac{1}{D|\Omega \setminus \Omega_\varepsilon|} \int_{\Omega \setminus \Omega_\varepsilon} u_0 + \varepsilon^2 u_2 \, d\mathbf{x}.$$

The challenge as before is to determine the correct expansion accurate to $\mathcal{O}(\varepsilon^2)$ by accounting for contributions from the inner expansion. We first decompose the region of integration $\Omega \setminus \Omega_\varepsilon := (\Omega \setminus B_\delta) \cup (B_\delta \setminus \Omega_\varepsilon)$ for the disk $B_\delta = \{\mathbf{x} \in \mathbb{R}^2 \mid |\mathbf{x} - \boldsymbol{\xi}| < \delta\}$ and then apply the limit $\delta \rightarrow 0$. The integral becomes

$$\int_{\Omega \setminus \Omega_\varepsilon} u \, d\mathbf{x} = \underbrace{\int_{B_\delta \setminus \Omega_\varepsilon} u \, d\mathbf{x}}_{I_1} + \underbrace{\int_{\Omega \setminus B_\delta} u \, d\mathbf{x}}_{I_2}.$$

The integral I_1 is evaluated by first transforming to the coordinate $\mathbf{y} = e^{-i\phi}(\mathbf{x} - \boldsymbol{\xi})/\varepsilon$ followed by $\mathbf{y} = \alpha\mathbf{z} + \beta/\mathbf{z}$ to find that

$$(2.54) \quad I_1 = \varepsilon^2 \int_{\substack{\mathbf{y} \in \mathbb{R}^2 \setminus \mathcal{A} \\ |\mathbf{y}| < \delta/\varepsilon}} U \, d\mathbf{y} = \frac{\varepsilon^2}{D} \int_{|\mathbf{z}|=1}^{|\mathbf{z}|=\delta/\varepsilon} \left(\underbrace{U_0}_{I_{10}} + \underbrace{\varepsilon U_1}_{I_{11}} + \underbrace{\varepsilon^2 U_2}_{I_{12}} + \cdots \right) |J| \, d\mathbf{z}.$$

From equation (2.24), we have that $U_0(\mathbf{z}) = S\nu \log |\mathbf{z}|$ so that for $\mathbf{z} = re^{i\theta}$,

$$(2.55) \quad \begin{aligned} I_{10} &= S\nu \varepsilon^2 \int_{\theta=0}^{2\pi} \int_{r=1}^{\frac{\delta}{\varepsilon}} \log r \left[\alpha^2 - \frac{2\alpha\beta}{r^2} \cos 2\theta + \frac{\beta^2}{r^4} \right] r \, dr \, d\theta = 2\pi S\nu \varepsilon^2 \int_{r=1}^{r=\frac{\delta}{\varepsilon}} \log r \left[\alpha^2 r + \frac{\beta^2}{r^3} \right] dr \\ &= 2\pi S\nu \varepsilon^2 \left[\alpha^2 \left(\frac{r^2}{2} \log r - \frac{r^2}{4} \right) - \beta^2 \left(\frac{1 + 2 \log r}{4r^2} \right) \right]_{r=1}^{r=\frac{\delta}{\varepsilon}} \approx \frac{S\nu\pi}{2} \left[2\delta^2 \log \frac{\delta}{\varepsilon\alpha} - \delta^2 + \varepsilon^2(\alpha^2 + \beta^2) \right]. \end{aligned}$$

Following on to the term I_{11} , we apply from (2.37) that $U_1 = -2\pi S\nu \mathbf{a} \cdot e^{-i\phi} v_{1c}$ where $v_{1c}(\mathbf{z}) = (\mathbf{z} - \mathbf{z}/|\mathbf{z}|^2)$. This leads to $I_{11} = \varepsilon^3 \int_{|\mathbf{z}|=1}^{|\mathbf{z}|=\delta/\varepsilon} U_1 |J| \, d\mathbf{z} = 0$. The contribution from $I_{22} = \mathcal{O}(\varepsilon^4)$.

The contribution from the outer region is now

$$(2.56) \quad I_2 = \int_{\Omega \setminus B_\delta} u \, d\mathbf{x} = \frac{1}{D} \underbrace{\int_{\Omega \setminus B_\delta} u_0 \, d\mathbf{x}}_{I_{20}} + \frac{\varepsilon^2}{D} \underbrace{\int_{\Omega \setminus B_\delta} u_2 \, d\mathbf{x}}_{I_{22}}.$$

The first term is calculated with $u_0 = -2\pi S\nu G(\mathbf{x}; \boldsymbol{\xi}) + \tau_0$ with $\tau_0 = S(1 + 2\pi\nu R(\boldsymbol{\xi}; \boldsymbol{\xi}))$ to determine

$$(2.57) \quad \begin{aligned} I_{20} &= \int_{\Omega \setminus B_\delta} u_0 \, d\mathbf{x} = \int_{\Omega} u_0 \, d\mathbf{x} - \int_{B_\delta} u_0 \, d\mathbf{x} \\ &= |\Omega| \tau_0 - \int_{B_\delta} [S\nu \log |\mathbf{x} - \boldsymbol{\xi}| + S] \, d\mathbf{x} - 2\pi S\nu \int_{B_\delta} (R(\mathbf{x}; \boldsymbol{\xi}) - R(\boldsymbol{\xi}; \boldsymbol{\xi})) \, d\mathbf{x} \\ &= |\Omega| \tau_0 - S\nu\pi\delta^2 \left(\log \delta - \frac{1}{2} \right) - S\pi\delta^2 + \mathcal{O}(\delta^4). \end{aligned}$$

Following on to the second term in (2.56), we calculate that

$$I_{22} = \int_{\Omega \setminus B_\delta} u_2 \, d\mathbf{x} = \int_{\Omega} u_2 \, d\mathbf{x} - \int_{B_\delta} u_2 \, d\mathbf{x}.$$

From (2.48b), the contributions of the second term have vanishing average, hence

$$\int_{B_\delta} u_2 \, d\mathbf{x} = \pi\delta^2 \frac{(a^2 + b^2)}{8}.$$

Combining (2.55) and (2.57), we have that

$$\begin{aligned}
\int_{\Omega \setminus \Omega_\varepsilon} u_0 + \varepsilon^2 u_2 d\mathbf{x} &= |\Omega| \tau_0 + \varepsilon^2 \left(\frac{S\nu\pi}{2} (\alpha^2 + \beta^2) + \int_{\Omega} u_2 d\mathbf{x} \right) + \mathcal{O}(\varepsilon^3), \\
(2.58) \quad &= |\Omega| \tau_0 + \varepsilon^2 |\Omega| \left(\frac{a^2 + b^2}{8} + \chi_2 + \int_{\Omega} \frac{1}{2} \text{Trace}(\mathcal{Q} \nabla_{\xi}^2 G(\mathbf{x}; \xi)) - 2\pi \mathbf{a} \cdot \mathcal{M} \nabla_{\xi} G(\mathbf{x}; \xi) d\mathbf{x} \right) + \mathcal{O}(\varepsilon^3).
\end{aligned}$$

Applying the identity (2.51), we note that the integral terms in (2.58) vanish since

$$(2.59) \quad \int_{\Omega} (G_{\xi_1 \xi_1} - G_{\xi_2 \xi_2}) d\mathbf{x} = 0, \quad \int_{\Omega} G_{\xi_1 \xi_2} d\mathbf{x} = 0, \quad \int_{\Omega} G_{\xi_1} d\mathbf{x} = 0, \quad \int_{\Omega} G_{\xi_2} d\mathbf{x} = 0.$$

Hence we obtain the final expression which incorporates the local and global contributions to the GMFPT,

$$(2.60) \quad \int_{\Omega \setminus \Omega_\varepsilon} u_0 + \varepsilon^2 u_2 d\mathbf{x} = |\Omega| \tau_0 + \varepsilon^2 |\Omega| \left(\frac{a^2 + b^2}{8} + \chi_2 \right).$$

Recalling the value of χ_2 given in (2.52), equation (2.58) then reduces to

$$(2.61) \quad \int_{\Omega \setminus \Omega_\varepsilon} u_0 + \varepsilon^2 u_2 d\mathbf{x} = |\Omega| \tau_0 + \varepsilon^2 |\Omega| \left(\frac{a^2 + b^2}{4} - |\Omega| \left(\text{Trace}(\mathcal{Q} \nabla_{\xi}^2 R(\xi; \xi)) + \pi \frac{(a+b)^2}{2} |\mathbf{a}|^2 - 2\pi \mathbf{a} \cdot \mathcal{Q} \mathbf{a} \right) \right).$$

Finally, using $|\Omega \setminus \Omega_\varepsilon| = |\Omega| - \pi \varepsilon^2 ab$, we have that

$$\begin{aligned}
\tau &= \frac{1}{D|\Omega \setminus \Omega_\varepsilon|} \int_{\Omega \setminus \Omega_\varepsilon} u_0 + \varepsilon^2 u_2 d\mathbf{x} = \frac{1}{D|\Omega|} \left[1 + \varepsilon^2 \frac{\pi ab}{|\Omega|} \right] \int_{\Omega \setminus \Omega_\varepsilon} u_0 + \varepsilon^2 u_2 d\mathbf{x} \\
(2.62) \quad &= \frac{\tau_0}{D} + \frac{\varepsilon^2}{D} \left(\frac{\pi ab}{|\Omega|} \tau_0 + \frac{a^2 + b^2}{4} - |\Omega| \left(\text{Trace}(\mathcal{Q} \nabla_{\xi}^2 R(\xi; \xi)) + \pi \frac{(a+b)^2}{2} |\mathbf{a}|^2 - 2\pi \mathbf{a} \cdot \mathcal{Q} \mathbf{a} \right) \right).
\end{aligned}$$

3. Results. In this section, we demonstrate the validity of the expansion and investigate how trap orientation modulates the GMFPT. In terms of minimizing the GMFPT, we remark that trap location is felt in the leading order through the term $R(\xi; \xi)$. Hence, when considering the role of orientation, we primarily focus on the correction terms $u_2(\mathbf{x})$ and τ_2 . A globally optimizing configuration of the GMFPT would first locate the trap at the critical points of τ_0 followed by choosing the orientation that optimizes τ_2 .

EXAMPLE 3.1. *Convergence in the disk geometry with a single elliptical trap.*

In this case where the enclosing geometry Ω is the unit disk, we have exact formula for the Green's function and we can obtain the necessary derivatives. From the equations (A.73), we calculate that

$$\begin{aligned}
\mathbf{a} = \nabla_{\xi} R(\xi; \xi) &= \frac{1}{2\pi} \frac{2 - |\xi|^2}{1 - |\xi|^2} \xi; \quad \text{Trace}(\mathcal{Q} \nabla_{\xi}^2 R(\xi; \xi)) = \frac{1}{\pi} \frac{\xi \cdot \mathcal{Q} \xi}{(1 - |\xi|^2)^2}; \quad \mathbf{a} \cdot \mathcal{Q} \mathbf{a} = \frac{1}{4\pi^2} \frac{(2 - |\xi|^2)^2}{(1 - |\xi|^2)^2} \xi \cdot \mathcal{Q} \xi; \\
(3.63) \quad S\nu &= \frac{|\Omega|}{2\pi} = \frac{1}{2}; \quad \tau_0 = \frac{|\Omega|}{2\pi\nu} \left[1 + 2\pi\nu R(\xi; \xi) \right] = \frac{1}{2} \left[\frac{1}{\nu} - \log(1 - |\xi|^2) + |\xi|^2 - \frac{3}{4} \right].
\end{aligned}$$

Applying (3) to (2.62) together with $|\Omega| = \pi$ and $D = 1$, yields the GMFPT

$$\begin{aligned}
\tau &= \tau_0 + \varepsilon^2 \left[ab\tau_0 + \frac{a^2 + b^2}{4} - \frac{(a+b)^2}{8} \left(\frac{2 - |\xi|^2}{1 - |\xi|^2} \right)^2 |\xi|^2 - \frac{2 - (2 - |\xi|^2)^2}{2(1 - |\xi|^2)^2} \xi \cdot \mathcal{Q} \xi \right] \\
(3.64) \quad &= \tau_0 + \varepsilon^2 \left[ab\tau_0 + \frac{a^2 + b^2}{4} - \frac{(a+b)^2}{8} \left(\frac{2 - |\xi|^2}{1 - |\xi|^2} \right)^2 |\xi|^2 + \frac{a^2 - b^2}{4} \frac{2 - (2 - |\xi|^2)^2}{2(1 - |\xi|^2)^2} \begin{bmatrix} \xi_1^2 - \xi_2^2 \\ 2\xi_1 \xi_2 \end{bmatrix} \cdot \begin{bmatrix} \cos 2\phi \\ \sin 2\phi \end{bmatrix} \right].
\end{aligned}$$

In Fig. 2, we show agreement between finite element solutions of (1.1) and the asymptotic result (3.64). The common variables in this validation are the disk geometry, the trap center $\xi = (0.3, 0.4)$ and the

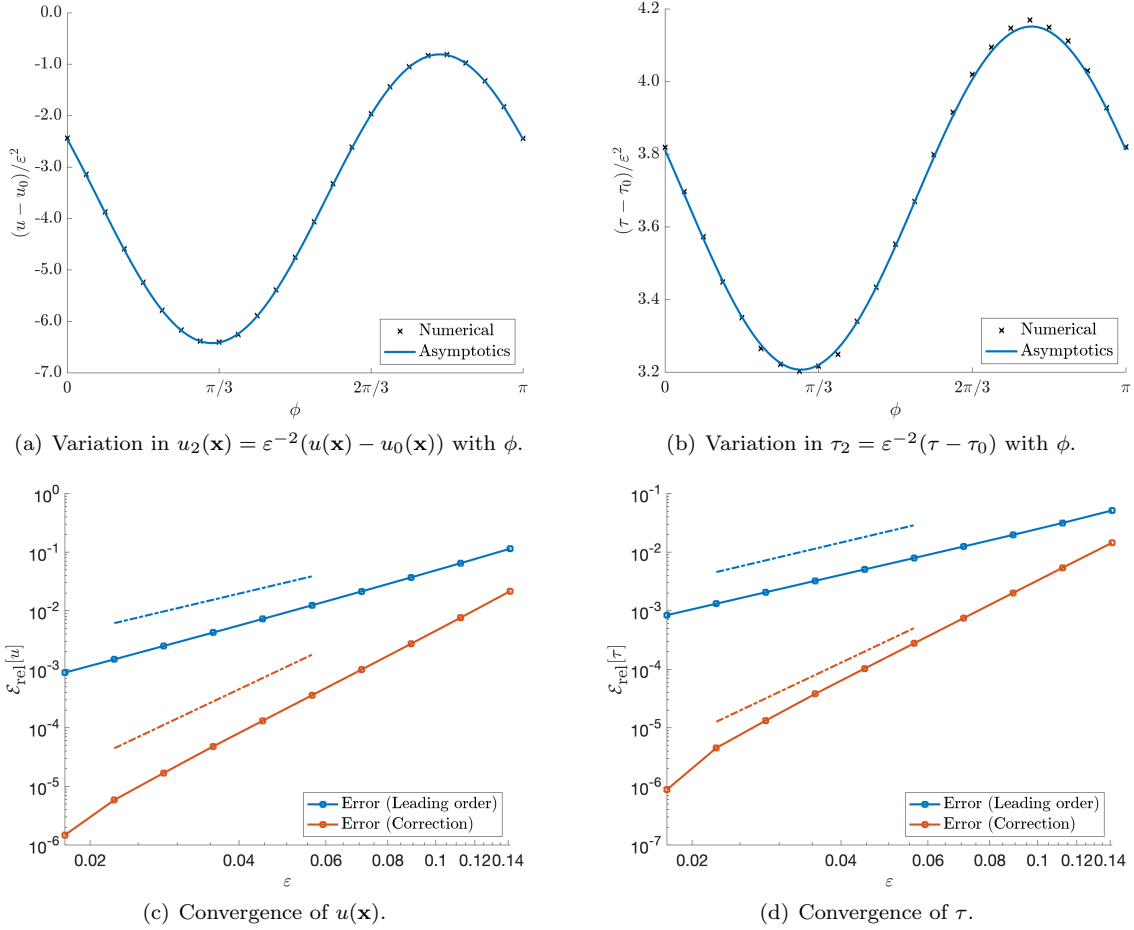


FIG. 2. Convergence of the asymptotic approximation (1.4) in the disk case with a trap centered at $\xi = (0.3, 0.4)$. Panel (a): Agreement between the solution correction $u_2(\mathbf{x}) = \varepsilon^{-2}(u(\mathbf{x}) - u_0(\mathbf{x}))$ for $\mathbf{x} = (-0.2, -0.4)$. Panel (b): The GMFPT correction $\tau_2 = \varepsilon^{-2}(\tau - \tau_0)$ from numerical and asymptotic approximations for $\varepsilon = 0.03$ as orientation ϕ varies. Panels (c-d): Convergence as $\varepsilon \rightarrow 0$ of the relative errors between numerical and asymptotic approximations (leading and correction) of $u(\mathbf{x})$ for $\mathbf{x} = (-0.2, -0.4)$ (c), and τ with fixed $\phi = \pi/6$ (d). Straight lines are of slope 2 (blue) and 4 (red) indicating convergence rates. Domain schematic shown in Fig. 3(a).

semi-axes dimensions $(a, b) = (3, 1)$. In Figs. 2(a)-2(b) we show agreement of the correction terms $u_2 = (u(\mathbf{x}) - u_0(\mathbf{x}))/\varepsilon^2$ at the point $\mathbf{x} = (-0.2, -0.4)$ and $\tau_2 = (\tau - \tau_0)/\varepsilon^2$ as the trap orientation ϕ varies with $\varepsilon = 0.03$ fixed. A schematic of the domain is shown in Fig. 3(a).

To directly confirm the convergence of the asymptotic expansion, we calculate a sequence of relative errors

$$(3.65) \quad \mathcal{E}_{\text{rel}}[z] = \left| \frac{z_{\text{approx}}(\varepsilon) - z_{\text{true}}}{z_{\text{true}}} \right|.$$

at a range of ε values. In (3.65) the true value is calculated from finite element simulations of (1.1) and the approximate values come from taking one or two terms in the expansion (1.4a). In Figs. 2(c)-2(d), we show that the rate of convergence in \mathcal{E}_{rel} as $\varepsilon \rightarrow 0^+$ is in agreement with the principal result (1.4), and in particular, the two term approximation (3.64) of the GMFPT has error $\mathcal{O}(\varepsilon^4)$.

EXAMPLE 3.2. Optimization of trap orientation for the GMFPT in the unit disk domain.

To study the optimizing trap orientations, we set $\xi = re^{i\theta}$ in (3.64) which reduces the GMFPT to

$$(3.66) \quad \tau \sim \tau_0 + \varepsilon^2 \left[ab\tau_0 + \frac{a^2 + b^2}{4} - \frac{(a+b)^2}{8} r^2 \left(\frac{2-r^2}{1-r^2} \right)^2 + \frac{a^2 - b^2}{4} g(r) \cos 2(\theta - \phi) \right], \quad g(r) = \frac{2 - (2-r^2)^2}{2(1-r^2)^2} r^2.$$

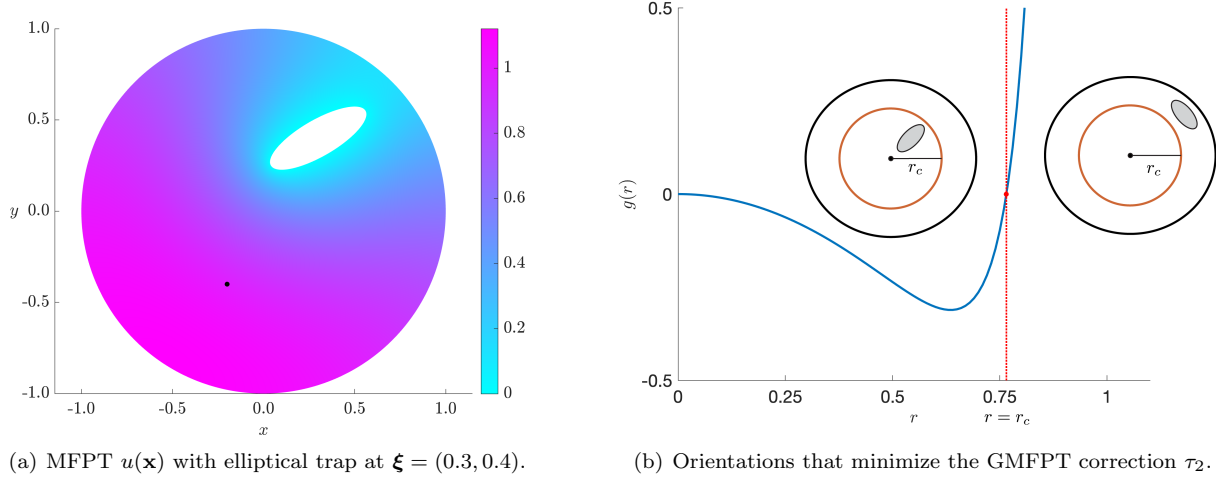


FIG. 3. Minimization of the GMFPT correction in the disk with a single elliptical trap. Panel (a): Domain with a single elliptical trap at $\xi = (0.3, 0.4)$, axes $\varepsilon(a, b) = \varepsilon(3, 1)$ and orientation $\phi = \pi/6$. The highlighted point (black dot) is $\mathbf{x} = (-0.2, -0.4)$. Panel (b): The function $g(r)$ and the critical radius $r = r_c$. For $r < r_c$, the GMFPT correction is minimized when the ellipse has major axis pointed towards the center of the disk.

The function $g(r)$ has the following (see Fig. 3(b)) simple properties,

$$g(r) \rightarrow 0^-, \quad \text{as } r \rightarrow 0^+; \quad g(r) \rightarrow +\infty, \quad \text{as } r \rightarrow 1^-; \quad g(r_c) = 0, \quad r_c = \sqrt{2 - \sqrt{2}},$$

and hence we can conclude that the correction τ_2 of the GMFPT is minimized when the semi-major axis of the trap is aligned in the radial direction, i.e. $\phi = \theta$, provided $g(r) < 0$ or $(2 - r^2)^2 > 2$. The GMFPT minimizing configuration is therefore

$$(3.67) \quad \phi = \begin{cases} \theta, & r \in (0, r_c), \\ \theta + \frac{\pi}{2}, & r \in (r_c, 1); \end{cases} \quad r_c = \sqrt{2 - \sqrt{2}} \approx 0.7654.$$

In Fig. 3(b), we plot the function $g(r)$ together with corresponding trap orientations that minimize the GMFPT. We also remark that the trap center which minimizes the leading order term τ_0 in GMFPT is $\xi = (0, 0)$. For a trap centered at this location, there is no contribution ($g(0) = 0$) to the GMFPT from the trap orientation as expected by symmetry considerations.

EXAMPLE 3.3. The MFPT from the origin to an elliptical trap in a disk.

In this example, we calculate the MFPT for a particle in the disk domain initially at $\mathbf{x} = 0$ to arrive at an elliptical trap centered at $\xi = re^{i\theta}$. From the main result (1.4c), we have the correction term

$$u_2(\mathbf{x}; \xi) = |\Omega| \left[\frac{1}{2} \text{Trace}(\mathcal{Q} \nabla_\xi^2 G(\mathbf{x}; \xi)) - 2\pi \nabla_\xi R(\xi; \xi) \cdot \mathcal{M} \nabla_\xi G(\mathbf{x}; \xi) \right] + \chi_2,$$

which describes the role that trap orientation plays in the capture rate. In Appendix A.1, we calculate the relevant terms to be

$$(3.68a) \quad \text{Trace}(\mathcal{Q} \nabla_\xi^2 G(\mathbf{0}; \xi)) = \frac{1}{\pi} \frac{\xi \cdot \mathcal{Q} \xi}{|\xi|^4};$$

$$(3.68b) \quad \nabla_\xi R(\xi; \xi) \cdot \mathcal{M} \nabla_\xi G(\mathbf{0}; \xi) = -\frac{1}{4\pi^2} \frac{2 - |\xi|^2}{|\xi|^2} \left[\xi \cdot \mathcal{Q} \xi - \frac{(a+b)^2}{4} |\xi|^2 \right].$$

We then have that

$$(3.68c) \quad u_2(\mathbf{0}) = \frac{a^2 + b^2}{8} - \frac{(a+b)^2}{8} \frac{(2-r^2)}{(1-r^2)^2} + \frac{a^2 - b^2}{8} \frac{2r^4 - 1}{r^2(1-r^2)^2} \cos(2(\phi - \theta)).$$

Favorable agreement between this result and numerical simulations is shown in Fig. 4. We conclude that $u_2(\mathbf{0})$ is minimized by orientating the trap in the radial direction ($\theta = \phi$) for $2r^4 - 1 < 0$ or $0 < r < 2^{-\frac{1}{4}} \approx 0.8409$. For $2^{-\frac{1}{4}} < r < 1$, $u_2(\mathbf{0})$ is minimized by orientating the semi-major axis of the trap parallel to the boundary.

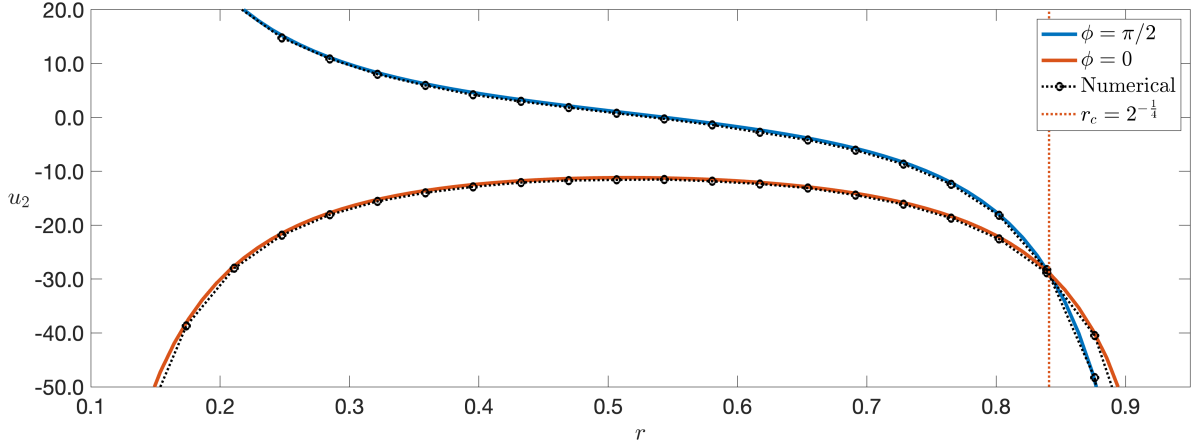


FIG. 4. The effects of trap orientation on the MFPT starting at the center of a disk. The correction $u_2 = \varepsilon^{-2}(u - u_0)$ from (3.68c) with a single trap of extent $\varepsilon = 0.01$, semi-major axes $(a, b) = (3, 1)$ centered at $\xi = (r, 0)$. Curves shown for orientations $\phi = \pi/2$ and $\phi = 0$.

EXAMPLE 3.4. Here we consider a general domain Ω with a single elliptical trap centered at $\mathbf{x} = \xi$ of semi-major and semi-minor axes εa and εb respectively and orientation ϕ with respect to the horizontal.

The GMFPT (2.61) reduces to the form

$$(3.69) \quad \tau = \tau_0 + \varepsilon^2 \left[\frac{\pi ab}{|\Omega|} \tau_0 + \frac{a^2 + b^2}{4} - \pi |\Omega| \frac{(a+b)^2}{2} (R_{\xi_1}^2 + R_{\xi_2}^2) + |\Omega| \frac{a^2 - b^2}{4} \mathbf{p} \cdot \begin{bmatrix} \cos 2\phi \\ \sin 2\phi \end{bmatrix} \right].$$

The vector \mathbf{p} is given as

$$(3.70) \quad \mathbf{p} = \begin{bmatrix} R_{\xi_1 \xi_1} - R_{\xi_2 \xi_2} - 2\pi(R_{\xi_1}^2 - R_{\xi_2}^2) \\ 2R_{\xi_1 \xi_2} - 4\pi R_{\xi_1} R_{\xi_2} \end{bmatrix} = \begin{bmatrix} R_{\xi_1 \xi_1} - R_{\xi_2 \xi_2} \\ 2R_{\xi_1 \xi_2} \end{bmatrix} - 2\pi \begin{bmatrix} R_{\xi_1}^2 - R_{\xi_2}^2 \\ 2R_{\xi_1} R_{\xi_2} \end{bmatrix}.$$

For some regular domains such as ellipses and rectangles, the function $R(\mathbf{x}; \xi)$ is available in the form of rapidly convergent series (see Appendices A.2 and A.3). The necessary derivatives $R_{\xi_1 \xi_1}, R_{\xi_2 \xi_2}, R_{\xi_1 \xi_2}, R_{\xi_1}$ and R_{ξ_2} in (3.70) can then be calculated by finite differences. We remark that if the trap center is chosen to optimize τ_0 , then we have $R_{\xi_1} = R_{\xi_2} = 0$ and so

$$(3.71) \quad \tau = \tau_0 + \varepsilon^2 \left[\frac{\pi ab}{|\Omega|} \tau_0 + \frac{a^2 + b^2}{4} + |\Omega| \frac{a^2 - b^2}{4} \begin{bmatrix} R_{\xi_1 \xi_1} - R_{\xi_2 \xi_2} \\ 2R_{\xi_1 \xi_2} \end{bmatrix} \cdot \begin{bmatrix} \cos 2\phi \\ \sin 2\phi \end{bmatrix} \right].$$

In Fig. 5 and Fig. 6, we plot vector fields of the orientation vector \mathbf{p} for the example of rectangular and elliptical domains, respectively. In each case, we form the necessary derivatives of $R(\mathbf{x}; \xi)$ by combining the rapidly convergent series stated in Appendix A together with centered finite difference approximations for the first and second derivatives. As the disk domain deforms into an ellipse, the bifurcation of the minimizing orientation noted in Fig. 3 is smoothed out. However, a generic observation remains that for traps centered close to a smooth boundary, τ_2 is minimized by orienting the semi-major axis of the trap parallel to $\partial\Omega$.

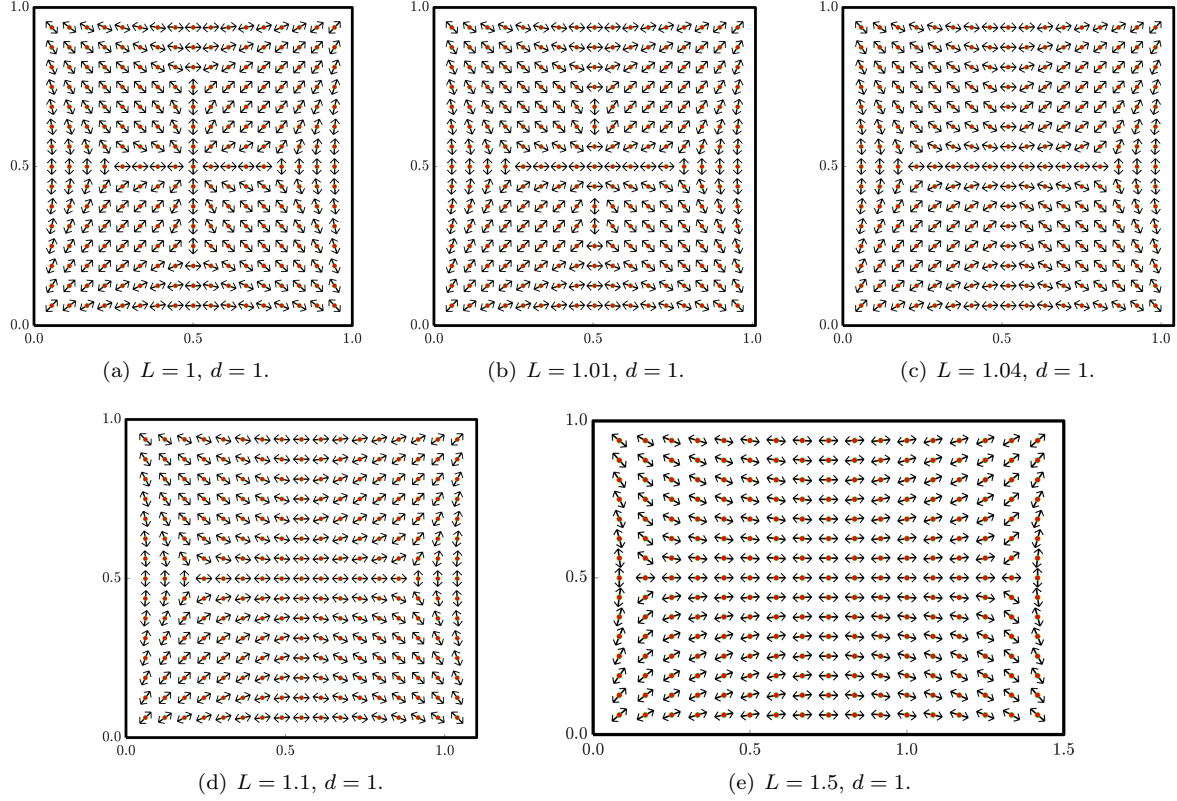


FIG. 5. Minimization of τ_2 for a single elliptical trap placed in the rectangular domain $\Omega = [0, L] \times [0, d]$ for $d = 1$ and $L = 1$ (a), $L = 1.01$ (b) $L = 1.02$ (c) $L = 1.04$ (d) $L = 1.1$ (e) $L = 1.5$. The directional arrow indicates the direction on which the semi-major axis should be aligned to minimize τ_2 , the higher order GMFPT correction term.

In the case of the rectangular domain $[0, L] \times [0, d]$, we observe similar discontinuous structures that deform from the square case ($L = d$) as the rectangle elongates ($L > d$). Curiously, the minimizing orientation of τ_2 at the corners is observed to be when the semi-major axis is aligned into the corners.

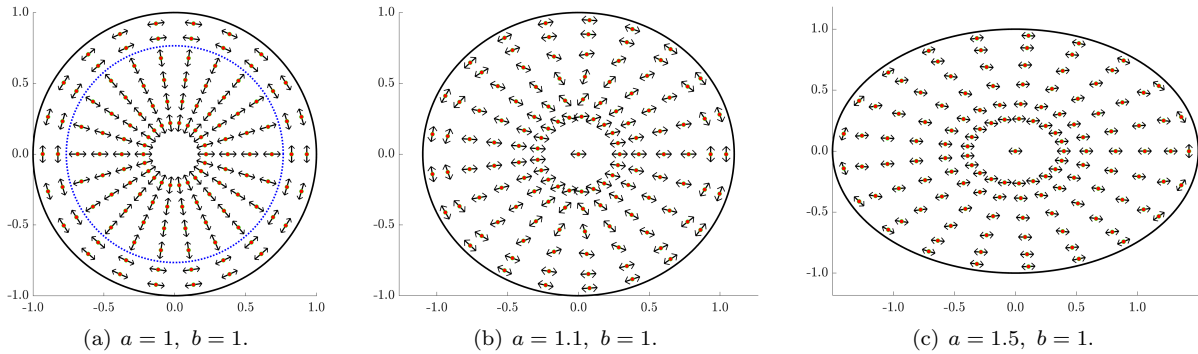


FIG. 6. Minimization of τ_2 for circular (a) and elliptical domains (b-c) at various locations. The directional arrow indicates the direction along which the semi-major axis should be aligned so that the correction term to the GMFPT is minimized. In Panel (a), the dashed blue line is the disk of radius $r_c = \sqrt{2 - \sqrt{2}} \approx 0.7654$ where the optimal orientation flips.

EXAMPLE 3.5. *The limit of an infinitely thin ellipse to a slit.*

In this example we consider the GMFPT in the limit as $b \rightarrow 0$ as the elliptical trap tends towards a thin

slit. The formula for the GMFPT is uniformly valid in this limit and we find from (3.69) that

$$(3.72) \quad \lim_{b \rightarrow 0^+} \tau = \tau_0 + \varepsilon^2 \left[\frac{a^2}{4} - \frac{\pi a^2 |\Omega|}{2} (R_{\xi_1}^2 + R_{\xi_2}^2) + \frac{a^2 |\Omega|}{4} \mathbf{p} \cdot \begin{bmatrix} \cos 2\phi \\ \sin 2\phi \end{bmatrix} \right].$$

In the case of a rectangular domain, we use this formula to explore the effect of trap orientation on the GMFPT. In Fig. 7 we display τ_2 for a trap with extent $\varepsilon = 0.2$, centered at $\boldsymbol{\xi} = [0.3, 0.4]$ inside the rectangular domain $\Omega = [0, 1] \times [0, 0.8]$. The two curves plotted are for trap orientations $\phi = \{\pi/2, \pi/6\}$ and for $a = 1$ and varying $0 < b < 1$. As expected, we see no effects of orientation when $a = b = 1$ and smooth behavior as $b \rightarrow 0$.

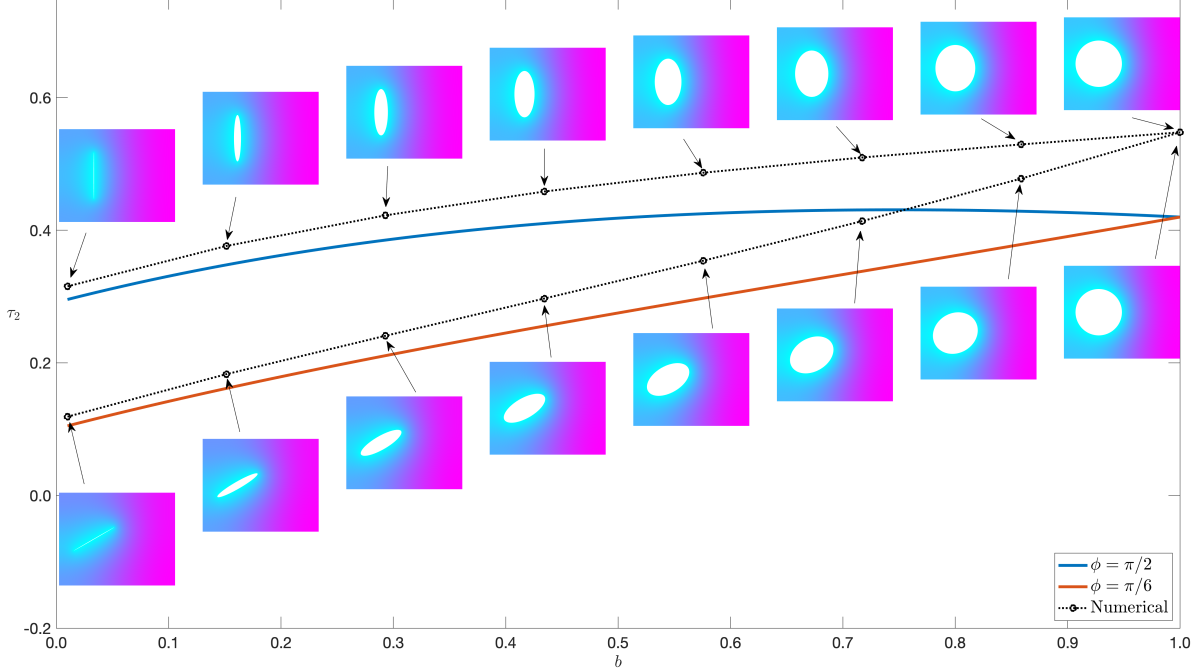


FIG. 7. The effects of trap orientation and ellipticity on the high order correction to the GMFPT in the limit as $b \rightarrow 0$. The correction $\tau_2 = \varepsilon^{-2}(\tau - \tau_0)$ to the GMFPT for a rectangular domain $\Omega = [0, 1] \times [0, 0.8]$ with a single trap of extent $\varepsilon = 0.2$, semi-major axis $a = 1$ centered at $\boldsymbol{\xi} = [0.3, 0.4]$ and varying semi-minor axis b . Curves shown for orientations $\phi = \pi/2$ and $\phi = \pi/6$ which coincide for circular traps ($b = 1$).

4. Discussion. In this work we have developed a high order matched asymptotic expansion for the MFPT of a Brownian walker to a small trap, enclosed in a two dimensional domain Ω . The high order correction term describes the effect that the orientation of the trap has on the capture rate. We investigated the role that trap orientation has on the MFPT and the GMFPT, observing a sensitive dependence on the centering point of the trap in the domain. In the specific case where the enclosing domain is a disk, we found a bifurcation where the correction to the GMFPT is minimized by orientating the semi-major axis of the trap in the radial direction when the centering point satisfies $0 < |\boldsymbol{\xi}| < \sqrt{2} - \sqrt{2}$, and is minimized by orientating in the angular direction when $\sqrt{2} - \sqrt{2} < |\boldsymbol{\xi}| < 1$ (Fig. 3). The discontinuous nature of this transition appears to be related to the symmetries of the domain and similar effects are noted in rectangular domains (Fig. 5). In domains with smooth boundaries, such as ellipses, we observe that the discontinuity in the vector field of optimal directions is smoothed out (Fig. 6). However, we observe that the GMFPT correction is generally minimized when the semi-major axis of the trap is aligned parallel to the boundary.

Our exposition of the role of trap orientation has focused on the case of an elliptical trap. This simple geometry allowed for explicit calculation of several key quantities, in particular the logarithmic capacitance d_c , the quadrupole matrix \mathcal{Q} and the moment polarization tensor \mathcal{M} . The determination of these key quantities was facilitated by a complex variable approach that utilized the known mapping between the disk

and ellipses to solve three variations of Laplace problems (Appendix B). However, our Principal Result (1.4), is valid for any trap geometry that features two lines of symmetry, for example those with rectangular or dumbbell shape. To apply the present results to these geometries, it would be necessary to calculate the three previously mentioned key quantities, either by a suitable complex transformation [22] or numerical method [2]. We hypothesize that the correction term derived in (1.4) would vanish for trap geometries with additional lines of symmetries, such as equilateral triangles or square. In such cases, further corrections would be necessary to describe the effects of orientation.

In future work, we aim to derive the MFPT in the presence of multiple absorbing elliptical bodies. This situation is relevant in the consideration of fly muscle cells which contain multiple well spaced nuclei of elliptical shape and correlated orientations [42]. This work shows the steps required to derive higher order corrections in a variety of narrow capture problems.

Acknowledgments. AEL acknowledges support from the NSF under award DMS 2052636.

Appendix A. Neumann Green's functions for disks, rectangles and ellipses. Here we state some known expressions for the Neumann Green's function (1.5) for the disk, ellipse and rectangle domains.

A.1. Neumann Green's function for a disk. In the case of the disk domain $\Omega = \{\mathbf{x} = (x_1, x_2) \mid x_1^2 + x_2^2 \leq 1\}$ and source $\boldsymbol{\xi} = (\xi_1, \xi_2)$, we have [22] that

$$G = \frac{-1}{2\pi} \log |\mathbf{x} - \boldsymbol{\xi}| + R(\mathbf{x}; \boldsymbol{\xi}); \quad R(\mathbf{x}; \boldsymbol{\xi}) = -\frac{1}{2\pi} \left[\frac{1}{2} \log(1 + |\mathbf{x}|^2 |\boldsymbol{\xi}|^2 - 2\mathbf{x} \cdot \boldsymbol{\xi}) - \frac{1}{2} (|\boldsymbol{\xi}|^2 + |\mathbf{x}|^2) + \frac{3}{4} \right].$$

We calculate gradients $\nabla_{\mathbf{x}} = (\partial_{x_1}, \partial_{x_2})$, $\nabla_{\boldsymbol{\xi}} = (\partial_{\xi_1}, \partial_{\xi_2})$ as

$$(A.73a) \quad \nabla_{\mathbf{x}} G = \frac{-1}{2\pi} \frac{\mathbf{x} - \boldsymbol{\xi}}{|\mathbf{x} - \boldsymbol{\xi}|^2} + \nabla_{\mathbf{x}} R; \quad \nabla_{\mathbf{x}} R = \frac{-1}{2\pi} \left[\frac{|\boldsymbol{\xi}|^2 \mathbf{x} - \boldsymbol{\xi}}{1 + |\mathbf{x}|^2 |\boldsymbol{\xi}|^2 - 2\mathbf{x} \cdot \boldsymbol{\xi}} - \mathbf{x} \right],$$

$$(A.73b) \quad \nabla_{\boldsymbol{\xi}} G = \frac{1}{2\pi} \frac{\mathbf{x} - \boldsymbol{\xi}}{|\mathbf{x} - \boldsymbol{\xi}|^2} + \nabla_{\boldsymbol{\xi}} R; \quad \nabla_{\boldsymbol{\xi}} R = \frac{-1}{2\pi} \left[\frac{|\mathbf{x}|^2 \boldsymbol{\xi} - \mathbf{x}}{1 + |\mathbf{x}|^2 |\boldsymbol{\xi}|^2 - 2\mathbf{x} \cdot \boldsymbol{\xi}} - \boldsymbol{\xi} \right].$$

As $\mathbf{x} \rightarrow \boldsymbol{\xi}$ we have

$$R(\boldsymbol{\xi}; \boldsymbol{\xi}) = \frac{-1}{2\pi} \left[\log(1 - |\boldsymbol{\xi}|^2) - |\boldsymbol{\xi}|^2 + \frac{3}{4} \right], \quad \nabla_{\boldsymbol{\xi}} R(\boldsymbol{\xi}; \boldsymbol{\xi}) = \frac{1}{2\pi} \left[\frac{2 - |\boldsymbol{\xi}|^2}{1 - |\boldsymbol{\xi}|^2} \right] \boldsymbol{\xi}.$$

The second derivatives for the Hessian are

$$(A.73c) \quad \frac{\partial^2 R}{\partial \xi_j^2} = \frac{-1}{2\pi} \left[\frac{|\mathbf{x}|^2 (1 + |\mathbf{x}|^2 |\boldsymbol{\xi}|^2 - 2\mathbf{x} \cdot \boldsymbol{\xi}) - 2(|\mathbf{x}|^2 \xi_j - x_j)^2}{(1 + |\mathbf{x}|^2 |\boldsymbol{\xi}|^2 - 2\mathbf{x} \cdot \boldsymbol{\xi})^2} - 1 \right], \quad \frac{\partial^2 R}{\partial \xi_1 \partial \xi_2} = \frac{1}{\pi} \frac{(|\mathbf{x}|^2 \xi_1 - x_1)(|\mathbf{x}|^2 \xi_2 - x_2)}{(1 + |\mathbf{x}|^2 |\boldsymbol{\xi}|^2 - 2\mathbf{x} \cdot \boldsymbol{\xi})^2},$$

$$(A.73d) \quad \frac{\partial^2 R}{\partial x_j^2} = \frac{-1}{2\pi} \left[\frac{|\boldsymbol{\xi}|^2 (1 + |\mathbf{x}|^2 |\boldsymbol{\xi}|^2 - 2\mathbf{x} \cdot \boldsymbol{\xi}) - 2(|\boldsymbol{\xi}|^2 x_j - \xi_j)^2}{(1 + |\mathbf{x}|^2 |\boldsymbol{\xi}|^2 - 2\mathbf{x} \cdot \boldsymbol{\xi})^2} - 1 \right], \quad \frac{\partial^2 R}{\partial x_1 \partial x_2} = \frac{1}{\pi} \frac{(|\boldsymbol{\xi}|^2 x_1 - \xi_1)(|\boldsymbol{\xi}|^2 x_2 - \xi_2)}{(1 + |\mathbf{x}|^2 |\boldsymbol{\xi}|^2 - 2\mathbf{x} \cdot \boldsymbol{\xi})^2}.$$

The terms $(R_{\xi_1 \xi_1} - R_{\xi_2 \xi_2})$ and $R_{\xi_1 \xi_2}$ as $\mathbf{x} \rightarrow \boldsymbol{\xi}$ are then

$$(A.73e) \quad \lim_{\mathbf{x} \rightarrow \boldsymbol{\xi}} \left(\frac{\partial^2 R}{\partial \xi_1^2} - \frac{\partial^2 R}{\partial \xi_2^2} \right) = \frac{1}{\pi} \frac{\xi_1^2 - \xi_2^2}{(1 - |\boldsymbol{\xi}|^2)^2}, \quad \lim_{\mathbf{x} \rightarrow \boldsymbol{\xi}} \frac{\partial^2 R}{\partial \xi_1 \partial \xi_2} = \frac{1}{\pi} \frac{\xi_1 \xi_2}{(1 - |\boldsymbol{\xi}|^2)^2}.$$

A.2. Neumann Green's function for a rectangle. The Green's function for a rectangle $\Omega = [0, L] \times [0, d]$ is known [10, 23] in the form of a rapidly convergent series. For $\mathbf{x} = (x_1, x_2)$ and $\boldsymbol{\xi} = (\xi_1, \xi_2)$ we have

$$\begin{aligned} R(\mathbf{x}; \boldsymbol{\xi}) &= \frac{-1}{2\pi} \sum_{n=0}^{\infty} \log(|1 - q^n z_{+,+}| |1 - q^n z_{+,-}| |1 - q^n z_{-,+}| |1 - q^n \zeta_{+,+}| |1 - q^n \zeta_{+,-}| |1 - q^n \zeta_{-,+}| |1 - q^n \zeta_{-,-}|) \\ (A.74a) \quad & - \frac{1}{2\pi} \log \frac{|1 - z_{-,-}|}{|r_{-,-}|} + \frac{L}{d} \left[\frac{1}{3} - \frac{\max(x_1, \xi_1)}{L} + \frac{x_1^2 + \xi_1^2}{2L^2} \right] - \frac{1}{2\pi} \sum_{n=1}^{\infty} \log |1 - q^n z_{-,-}|. \end{aligned}$$

where

$$(A.74b) \quad z_{\pm,\pm} \equiv e^{\mu r_{\pm,\pm}/2}, \quad \zeta_{\pm,\pm} \equiv e^{\mu \rho_{\pm,\pm}/2}, \quad \mu \equiv \frac{2\pi}{d}, \quad q \equiv e^{-\mu L},$$

$$(A.74c) \quad r_{+,\pm} \equiv -|x_1 + \xi_1| + i(x_2 \pm \xi_2), \quad r_{-,\pm} \equiv -|x_1 - \xi_1| + i(x_2 \pm \xi_2),$$

$$(A.74d) \quad \rho_{+,\pm} \equiv |x_1 + \xi_1| + i(x_2 \pm \xi_2) - 2L, \quad \rho_{-,\pm} \equiv |x_1 - \xi_1| + i(x_2 \pm \xi_2) - 2L.$$

The self interaction term $R(\mathbf{x}; \mathbf{x})$ is given by

$$\begin{aligned} R(\mathbf{x}; \mathbf{x}) &= \frac{-1}{2\pi} \sum_{n=0}^{\infty} \log(|1 - q^n z_{+,+}^0| |1 - q^n z_{+,-}^0| |1 - q^n z_{-,+}^0| |1 - q^n \zeta_{+,+}^0| |1 - q^n \zeta_{+,-}^0| |1 - q^n \zeta_{-,+}^0| |1 - q^n \zeta_{-,-}^0|) \\ (A.75a) \quad & + \frac{L}{d} \left(\frac{1}{3} - \frac{x_1}{L} + \frac{x_1^2}{L^2} \right) - \frac{1}{2\pi} \log \left(\frac{\pi}{d} \right) - \frac{1}{2\pi} \sum_{n=1}^{\infty} \log(1 - q^n). \end{aligned}$$

where

$$(A.75b) \quad z_{+,+}^0 \equiv e^{\mu(-x_1 + ix_2)}, \quad z_{+,-}^0 \equiv e^{-\mu x_1}, \quad z_{-,+}^0 \equiv e^{\mu ix_2},$$

$$(A.75c) \quad \zeta_{+,+}^0 \equiv e^{\mu(x_1 - L + ix_2)}, \quad \zeta_{+,-}^0 \equiv e^{\mu(-L + ix_2)}, \quad \zeta_{-,+}^0 \equiv e^{\mu(x_1 - L)}, \quad \zeta_{-,-}^0 \equiv e^{-\mu L}.$$

A.3. Neumann Green's function for an ellipse. A rapidly convergent series for the solution of (1.5) in the elliptical domain $\Omega = \{\mathbf{x} = (x_1, x_2) \mid (x_1/a)^2 + (x_2/b)^2 \leq 1\}$ was derived in [19]. For completeness we restate the final result here. The first step is to introduce the transformation,

$$(A.76a) \quad x_1 = f \cosh \xi \cos \eta, \quad x_2 = f \sinh \xi \sin \eta, \quad f = \sqrt{a^2 - b^2},$$

which maps $\mathbf{x} = (x_1, x_2) \in \Omega$ to the rectangle $0 \leq \xi \leq \xi_b$ and $0 \leq \eta \leq 2\pi$ where $a = f \cosh \xi_b$ and $b = f \sinh \xi_b$ so that

$$(A.76b) \quad f = \sqrt{a^2 - b^2}, \quad \xi_b = \tanh^{-1} \frac{b}{a} = -\frac{1}{2} \log \gamma, \quad \gamma = \left(\frac{a-b}{a+b} \right).$$

For a pair (x_1, x_2) , the corresponding (ξ, η) satisfy

$$\xi = \frac{1}{2} \log \left(1 - 2s + s\sqrt{s^2 - 1} \right), \quad s = \frac{-\mu - \sqrt{\mu^2 + 4f^2 y^2}}{2f^2}, \quad \mu = x_1^2 + x_2^2 - f^2.$$

For $\eta_* = \sin^{-1}(\sqrt{p})$, the value of η is given by

$$(A.76c) \quad \eta = \begin{cases} \eta_*, & \text{for } x_1 \geq 0, x_2 \geq 0 \\ \pi - \eta_*, & \text{for } x_1 < 0, x_2 \geq 0 \\ \pi + \eta_*, & \text{for } x_1 \leq 0, x_2 < 0 \\ 2\pi - \eta_*, & \text{for } x_1 > 0, x_2 < 0 \end{cases}, \quad \text{where} \quad p = \frac{-\mu + \sqrt{\mu^2 + 4f^2 y^2}}{2f^2}.$$

For points $\mathbf{x} = (x_1, x_2)$ and $\mathbf{y} = (y_1, y_2)$, the Green's function $G(\mathbf{x}; \mathbf{y})$ for $\mathbf{x} \neq \mathbf{y}$ is given by

$$(A.77) \quad G(\mathbf{x}; \mathbf{y}) = \frac{1}{4|\Omega|}(|\mathbf{x}|^2 + |\mathbf{y}|^2) - \frac{3}{16|\Omega|}(a^2 + b^2) - \frac{1}{4\pi} \log \gamma - \frac{1}{2\pi} \max(\xi, \xi_0) - \frac{1}{2\pi} \sum_{n=0}^{\infty} \log \left(\prod_{j=1}^8 |1 - \gamma^{2n} z_j| \right),$$

where $|\Omega| = \pi ab$. The complex constants z_1, \dots, z_8 are defined in terms of (ξ, η) , (ξ_0, η_0) and ξ_b by

$$\begin{aligned} z_1 &= e^{-|\xi - \xi_0| + i(\eta - \eta_0)}, & z_2 &= e^{|\xi - \xi_0| - 4\xi_b + i(\eta - \eta_0)}, & z_3 &= e^{(\xi + \xi_0) - 2\xi_b + i(\eta - \eta_0)}, \\ z_4 &= e^{(\xi + \xi_0) - 2\xi_b + i(\eta - \eta_0)}, & z_5 &= e^{(\xi + \xi_0) - 4\xi_b + i(\eta + \eta_0)}, & z_6 &= e^{-(\xi + \xi_0) + i(\eta + \eta_0)}, \\ z_7 &= e^{|\xi + \xi_0| - 2\xi_b + i(\eta + \eta_0)}, & z_8 &= e^{-|\xi + \xi_0| - 2\xi_b + i(\eta + \eta_0)}. \end{aligned}$$

The point (x_1, x_2) is mapped to (ξ, η) while the source point (y_1, y_2) is mapped to (ξ_0, η_0) by the transformation (A.76). The quantity $R(\mathbf{y}; \mathbf{y})$ is given by

$$\begin{aligned} R(\mathbf{y}; \mathbf{y}) &= \frac{|\mathbf{y}|^2}{2|\Omega|} - \frac{3}{16|\Omega|}(a^2 + b^2) + \frac{1}{2\pi} \log(a + b) - \frac{\xi_0}{2\pi} + \frac{1}{4\pi} \log(\cosh^2 \xi_0 - \cos^2 \eta_0) \\ &\quad - \frac{1}{2\pi} \sum_{n=1}^{\infty} \log(1 - \gamma^{2n}) - \frac{1}{2\pi} \sum_{n=0}^{\infty} \log \left(\prod_{j=2}^8 |1 - \gamma^{2n} z_j^0| \right) \end{aligned}$$

Here the constants z_j^0 for $j = 2, \dots, 8$ are

$$\begin{aligned} z_2^0 &= \gamma^2, & z_3^0 &= \gamma e^{-2\xi_0}, & z_4^0 &= \gamma e^{2\xi_0}, & z_4^0 &= \gamma^2 e^{2\xi_0 + 2i\eta_0}, \\ z_6^0 &= e^{-2\xi_0 + 2i\eta_0}, & z_7^0 &= \gamma e^{2i\eta_0}, & z_8^0 &= \gamma e^{2i\eta_0}, & \gamma &= \frac{a - b}{a + b}. \end{aligned}$$

Appendix B. Inner problems for the exterior of the ellipse.

We solve a variety of Laplace equations posed in the exterior of the elliptical domain $\mathcal{A} = \{\mathbf{y} = (y_1, y_2) \mid y_1^2/a^2 + y_2^2/b^2 < 1\}$. In each case, we make use of the complex transformation

$$(B.78) \quad \mathbf{y} = \alpha \mathbf{z} + \frac{\beta}{\mathbf{z}},$$

which maps the unit disk to the ellipse \mathcal{A} with semi-major and semi-minor axes a and b respectively with the semi-major axis aligned on the horizontal axis. On the unit disk $\mathbf{z} = e^{i\theta}$, we have that

$$\mathbf{y} = \alpha e^{i\theta} + \beta e^{-i\theta} = (\alpha + \beta) \cos \theta + i(\alpha - \beta) \sin \theta = a \cos \theta + ib \sin \theta.$$

The mapping parameters α and β are then

$$(B.79) \quad \alpha = \frac{a + b}{2}, \quad \beta = \frac{a - b}{2}.$$

The Laplace equations to be considered will be solved in the unit disk then mapped to the ellipse by the inverse transformation of (B.78). The large argument behavior of the inverse transform of (B.78) is calculated as follows for $|\mathbf{y}| \gg 1$

$$(B.80) \quad \mathbf{z} \sim \frac{\mathbf{y}}{\alpha} - \frac{\beta}{\mathbf{y}} = \frac{\mathbf{y}}{\alpha} - \frac{\beta \bar{\mathbf{y}}}{|\mathbf{y}|^2}, \quad |\mathbf{z}| = \frac{|\mathbf{y}|}{\alpha} \left[1 - \frac{\alpha \beta}{|\mathbf{y}|^4} \mathbf{y}^T \begin{pmatrix} 1 & 0 \\ 0 & -1 \end{pmatrix} \mathbf{y} + \mathcal{O}(|\mathbf{y}|^{-4}) \right], \quad |\mathbf{y}| \rightarrow \infty.$$

B.1. The order $\mathcal{O}(\varepsilon^0)$ problem. The leading order inner problem is given by

$$(B.81a) \quad \Delta_{\mathbf{y}} v_{0c} = 0, \quad \mathbf{y} \in \mathbb{R}^2 \setminus \mathcal{A}; \quad v_{0c} = 0, \quad \mathbf{y} \in \partial \mathcal{A};$$

$$(B.81b) \quad v_{0c} = \log |\mathbf{y}| - \log d_c + \frac{\mathbf{d} \cdot \mathbf{y}}{|\mathbf{y}|^2} + \frac{\mathbf{y}^T \tilde{\mathcal{Q}} \mathbf{y}}{|\mathbf{y}|^4} + \dots \quad |\mathbf{y}| \rightarrow \infty.$$

In classic potential theory, the logarithmic term is the monopole, \mathbf{d} is the dipole vector and $\tilde{\mathbf{Q}}$ is the quadrupole matrix. Our goal is to obtain the solution of (B.81) and identify the logarithmic capacitance d_c and quadrupole matrix $\tilde{\mathbf{Q}}$. In the scenario of the unit disk ($a = b = 1$), the unique solution is $\log |\mathbf{z}|$. For the problem (B.81), we apply the mapping (B.80) to obtain the far field behavior

$$(B.82) \quad v_{0c}(\mathbf{y}) = \log |\mathbf{z}| \sim \log |\mathbf{y}| - \log \alpha - \frac{\alpha\beta}{|\mathbf{y}|^4} \mathbf{y}^T \begin{pmatrix} 1 & 0 \\ 0 & -1 \end{pmatrix} \mathbf{y} + \mathcal{O}(|\mathbf{y}|^{-4}).$$

Hence in comparing (B.81b) with (B.82), and applying (B.79), we establish that

$$(B.83) \quad d_c = \log \frac{a+b}{2}, \quad \mathbf{d} = \mathbf{0}, \quad \tilde{\mathbf{Q}} = -\alpha\beta \begin{pmatrix} 1 & 0 \\ 0 & -1 \end{pmatrix} = -\frac{a^2 - b^2}{4} \begin{pmatrix} 1 & 0 \\ 0 & -1 \end{pmatrix}.$$

The vanishing dipole vector $\mathbf{d} = 0$ is consistent with the two lines of symmetry of the elliptical domain. Extending this analogy, domains with four lines of symmetries (e.g. square) would have a vanishing quadrupole matrix requiring an even higher order of expansion.

B.2. The order $\mathcal{O}(\varepsilon^1)$ problem. The first order inner problem is vector valued and given by

$$(B.84a) \quad \Delta_{\mathbf{y}} \mathbf{v}_{1c} = 0, \quad \mathbf{y} \in \mathbb{R}^2 \setminus \mathcal{A}; \quad \mathbf{v}_{1c} = 0, \quad \mathbf{y} \in \partial\mathcal{A};$$

$$(B.84b) \quad \mathbf{v}_{1c} = \mathbf{y} + \frac{\tilde{\mathcal{M}}\mathbf{y}}{|\mathbf{y}|^2} + \dots \quad |\mathbf{y}| \rightarrow \infty.$$

For the case of the unit disk, we have that $\mathbf{v}_{1d} = \mathbf{z} - \mathbf{z}/|\mathbf{z}|^2$. Hence for the elliptical domain under the transformation (B.80), we have that

$$(B.85) \quad \mathbf{v}_{1c}(\mathbf{y}) = \alpha \mathbf{v}_{1d}(\mathbf{y}) = \mathbf{y} + \frac{\tilde{\mathcal{M}}\mathbf{y}}{|\mathbf{y}|^2} + \dots \quad |\mathbf{y}| \rightarrow \infty; \quad \tilde{\mathcal{M}} = -\alpha \begin{pmatrix} a & 0 \\ 0 & b \end{pmatrix}.$$

B.3. The order $\mathcal{O}(\varepsilon^2)$ problem. In this subsection, we derive the solution of the higher order correction problem

$$(B.86a) \quad \Delta_{\mathbf{y}} v_{2c} = -1, \quad \mathbf{y} \in \mathbb{R}^2 \setminus \mathcal{A}; \quad v_{2c} = 0, \quad \mathbf{y} \in \partial\mathcal{A};$$

$$(B.86b) \quad v_{2c} = -\frac{|\mathbf{y}|^2}{4} + \mathbf{y}^T \mathcal{B} \mathbf{y} + \dots \quad |\mathbf{y}| \rightarrow \infty, \quad \mathcal{B} = \begin{bmatrix} \mathcal{B}_{11} & \mathcal{B}_{12} \\ \mathcal{B}_{12} & -\mathcal{B}_{11} \end{bmatrix}.$$

where $\text{Trace}(\mathcal{B}) = 0$. The general solution takes the form $v_{2c} = -\frac{1}{4}|\mathbf{y}|^2 + v_{2h}$ where the homogeneous solution satisfies

$$(B.87a) \quad \Delta_{\mathbf{y}} v_{2h} = 0, \quad \mathbf{y} \in \mathbb{R}^2 \setminus \mathcal{A}; \quad v_{2h} = \frac{|\mathbf{y}|^2}{4}, \quad \mathbf{y} \in \partial\mathcal{A};$$

$$(B.87b) \quad v_{2h} \sim \mathbf{y}^T \mathcal{B} \mathbf{y} + \dots \quad |\mathbf{y}| \rightarrow \infty.$$

As with previous solutions of inner problems, we solve the corresponding problem on the disk and use the complex transformation (B.78) to map the solution to \mathcal{A} . Recalling that when $\mathbf{z} = e^{i\theta}$, we have $|\mathbf{y}|^2 = (\alpha^2 + \beta^2) + 2\alpha\beta \cos 2\theta$. Hence, the homogeneous solutions is expressed in terms of the disk solution in complex form as

$$(B.88) \quad v_{2h} = a_1 + \text{Re}[b_1 \mathbf{z}^2 + b_2 \mathbf{z}^{-2}] + \text{Im}[c_1 \mathbf{z}^2 + c_2 \mathbf{z}^{-2}].$$

On the boundary $\mathbf{z} = e^{i\theta}$, we have the conditions

$$\frac{1}{4}(\alpha^2 + \beta^2) + \frac{1}{2}\alpha\beta \cos 2\theta = a_1 + (b_1 + b_2) \cos 2\theta + (c_1 + c_2) \sin 2\theta,$$

which yields the conditions

$$a_1 = \frac{1}{4}(\alpha^2 + \beta^2), \quad b_1 + b_2 = \frac{1}{2}\alpha\beta, \quad c_1 + c_2 = 0.$$

To establish the behavior as $|\mathbf{y}| \rightarrow \infty$, we consider from (B.80) that

$$\mathbf{z}^2 \sim \left(\frac{\mathbf{y}}{\alpha} - \frac{\beta}{\mathbf{y}} \right)^2 = \frac{\mathbf{y}^2}{\alpha^2} - 2\frac{\beta}{\alpha} + \frac{\beta^2}{\mathbf{y}^2}, \quad \text{as } |\mathbf{y}| \rightarrow \infty.$$

The large argument behavior of v_{2h} given in (B.88) is

$$v_{2h} \sim \frac{b_1}{\alpha^2} \text{Re}[\mathbf{y}^2] + \frac{c_1}{\alpha^2} \text{Im}[\mathbf{y}^2] + \frac{1}{4}(\alpha^2 + \beta^2) - 2\frac{\beta}{\alpha}b_1 + \mathcal{O}(|\mathbf{y}|^{-2}).$$

Now, comparing with (B.87b), we see that

$$(B.89) \quad b_1 = \alpha^2 \mathcal{B}_{11}, \quad c_1 = \alpha^2 \mathcal{B}_{12}.$$

Hence, we obtain the large argument behavior of (B.87) to be

$$(B.90a) \quad v_{2h} \sim \mathbf{y}^T \mathcal{B} \mathbf{y} + \frac{1}{4}(\alpha^2 + \beta^2) - 2\alpha\beta \mathcal{B}_{11} + \mathcal{O}(|\mathbf{y}|^{-2}),$$

and finally establish the large argument behavior of (B.86) to be

$$(B.91) \quad v_{2c} = -\frac{|\mathbf{y}|^2}{4} + \mathbf{y}^T \mathcal{B} \mathbf{y} + d_{2c} + \mathcal{O}(|\mathbf{y}|^{-2}), \quad \text{as } |\mathbf{y}| \rightarrow \infty; \quad d_{2c} = \frac{1}{4}(\alpha^2 + \beta^2) - 2\alpha\beta \mathcal{B}_{11}.$$

References.

- [1] D. AMBROSI, A. GAMBA, AND G. SERINI, *Cell directional and chemotaxis in vascular morphogenesis*, Bull. Math. Biol., 66 (2004), pp. 1851–1873.
- [2] PETER BADDIO AND LLOYD N. TREFETHEN, *Log-lightning computation of capacity and green's function*, Maple Transactions, 1 (2021).
- [3] A.J. BERNOFF, A. JILKINE, A. NAVARRO HERNÁNDEZ, AND A.E. LINDSAY, *Single-cell directional sensing from just a few receptor binding events*, Biophys. J., 122 (2023), pp. 3108–3116.
- [4] ANDREW J. BERNOFF AND ALAN E. LINDSAY, *Kinetic monte carlo methods for three-dimensional diffusive capture problems in exterior domains*, Royal Society Open Science, 12 (2025), p. 241033.
- [5] P.C. BRESSLOFF AND J.M. NEWBY, *Stochastic models of intracellular transport*, Rev. Mod. Phys., 85 (2013), pp. 135–196.
- [6] P.C. BRESSLOFF AND R.D. SCHUMM, *The narrow capture problem with partially absorbing targets and stochastic resetting*, Multiscale Model. Simul., 20 (2022), pp. 857–881.
- [7] PAUL C BRESSLOFF, *Asymptotic analysis of particle cluster formation in the presence of anchoring sites.*, Eur Phys J E Soft Matter, 47 (2024), p. 30.
- [8] PAUL C. BRESSLOFF, *Cellular diffusion processes in singularly perturbed domains*, Journal of Mathematical Biology, 89 (2024), p. 58.
- [9] ALAIN CAMPBELL AND SERGUEÏ NAZAROV, *An asymptotic study of a plate problem by a rearrangement method. application to the mechanical impedance*, ESAIM: Mathematical Modelling and Numerical Analysis - Modélisation Mathématique et Analyse Numérique, 32 (1998), pp. 579–610.
- [10] W. CHEN AND M. J. WARD, *The stability and dynamics of localized spot patterns in the two-dimensional gray-scott model*, SIAM Journal on Applied Dynamical Systems, 10 (2011), pp. 582–666.
- [11] P. FAUCHALD AND T. TORKILD, *Using first-passage time in the analysis of area-restricted search and habitat selection*, Ecology, 84 (2003), pp. 282–288.
- [12] K.R. GHUSINGA, J.J. DENNEHY, AND A. SINGH, *First-passage time approach to controlling noise in the timing of intracellular events*, Proc. Natl. Acad. Sci., 114 (2017), pp. 693–698.
- [13] M.M. GIBBONS, T. CHOU, AND M.R. D'ORSOGNA, *Diffusion-dependent mechanisms of receptor engagement and viral entry*, J. Phys. Chem. B, 114 (2010), pp. 15403–15412.

- [14] DENIS GREBENKOV, RALF METZLER, AND GLEB OSHANIN, eds., *Target Search Problems*, Springer International Publishing, Cham, 2024.
- [15] DENIS S GREBENKOV, RALF METZLER, AND GLEB OSHANIN, *Effects of the target aspect ratio and intrinsic reactivity onto diffusive search in bounded domains*, New Journal of Physics, 19 (2017), p. 103025.
- [16] D. HOLCMAN AND Z. SCHUSS, *The narrow escape problem*, SIAM Review, 56 (2014), pp. 213–257.
- [17] SAMUEL A. ISAACSON AND JAY NEWBY, *Uniform asymptotic approximation of diffusion to a small target*, Phys. Rev. E, 88 (2013), p. 012820.
- [18] SARAFA IYANIWURA, TONY WONG, MICHAEL J. WARD, AND COLIN B. MACDONALD, *Simulation and optimization of mean first passage time problems in 2-d using numerical embedded methods and perturbation theory*, Multiscale Modeling & Simulation, 19 (2021), pp. 1367–1393.
- [19] SARAFA A. IYANIWURA, TONY WONG, COLIN B. MACDONALD, AND MICHAEL J. WARD, *Optimization of the mean first passage time in near-disk and elliptical domains in 2-d with small absorbing traps*, SIAM Review, 63 (2021), pp. 525–555.
- [20] KURMANBEK KAIYRBEKOV AND BRIAN A. CAMLEY, *Does nematic order allow groups of elongated cells to sense electric fields better?*, 2024.
- [21] T. KOLOKOLNIKOV AND AE LINDSAY, *Recovering multiple small inclusions in a three-dimensional domain using a single measurement*, Inverse Problems in Science and Engineering, 23 (2015), pp. 377–388.
- [22] T. KOLOKOLNIKOV, M. S. TITCOMBE, AND M. J. WARD, *Optimizing the fundamental neumann eigenvalue for the laplacian in a domain with small traps*, European Journal of Applied Mathematics, 16 (2005), p. 161–200.
- [23] T. KOLOKOLNIKOV, M.J. WARD, AND J. WEI, *Spot self-replication and dynamics for the schnakenburg model*, J. Nonlinear Science, 19 (2009), pp. 302–332.
- [24] MC KROPINSKI, AE LINDSAY, AND MJ WARD, *Asymptotic analysis of localized solutions to some linear and nonlinear biharmonic eigenvalue problems*, Studies in Applied Mathematics, 126 (2011), pp. 347–408.
- [25] V. KURELLA, JC. TZOU, D. COOMBS, AND MJ. WARD, *Asymptotic analysis of first passage time problems inspired by ecology*, Bull. Math. Biol., 77 (2015), pp. 83–125.
- [26] SD. LAWLEY, AE. LINDSAY, AND CE. MILES, *Receptor organization determines the limits of single-cell source location detection*, Phys. Rev. Lett., 125 (2020), p. 018102.
- [27] VIVienne LEECH, MOHIT P. DALWADI, AND ANGELIKA MANHART, *A dynamical analysis of the alignment mechanism between two interacting cells*, Bulletin of Mathematical Biology, 87 (2025), p. 23.
- [28] V. LEECH, J.W. HAZEL, J.C. GATLIN, A.E. LINDSAY, AND A. MANHART, *Mathematical modeling accurately predicts the dynamics and scaling of nuclear growth in discrete cytoplasmic volumes*, Journal of Theoretical Biology, 533 (2022), p. 110936.
- [29] AE. LINDSAY, AJ. BERNOFF, AND A. NAVARRO HERNÁNDEZ, *Short-time diffusive fluxes over membrane receptors yields the direction of a signalling source*, R. Soc. Open Sci., 10 (2023), p. 221619.
- [30] AE. LINDSAY, T. KOLOKOLNIKOV, AND JC. TZOU, *Narrow escape problem with a mixed trap and the effect of orientation*, Phys. Rev. E, 91 (2015), p. 032111.
- [31] A.E. LINDSAY, B. QUAIFFE, AND L. WENDELBERGER., *A boundary element method for computing the vibrational modes of elastic plates with localized punctures.*, Advances in Computation, 44 (2018), pp. 1249–1273.
- [32] A. E. LINDSAY, W. HAO, AND A. J. SOMMESE, *Vibrations of thin plates with small clamped patches*, Proceedings of the Royal Society of London A: Mathematical, Physical and Engineering Sciences, 471 (2015).
- [33] A. E. LINDSAY, M. J. WARD, AND T. KOLOKOLNIKOV, *The transition to a point constraint in a mixed biharmonic eigenvalue problem*, SIAM Journal on Applied Mathematics, 75 (2015), pp. 1193–1224.
- [34] RALF METZLER, GLEB OSHANIN, AND SIDNEY REDNER, *First-Passage Phenomena and Their Applications*, WORLD SCIENTIFIC, 2014.
- [35] J. MORGAN AND AE. LINDSAY, *Modulation of antigen discrimination by duration of immune contacts in a kinetic proofreading model of T cell activation with extreme statistics*, PLOS Comp. Biol., 19 (2023), pp. 1–17.
- [36] JONATHAN MORGAN, JOHANNES PETTMANN, OMER DUSHEK, AND ALAN E. LINDSAY, *T cell microvilli simulations show operation near packing limit and impact on antigen recognition*, Biophysical

- Journal, 121 (2022), pp. 4128–4136.
- [37] KENTO NAKAMURA AND TETSUYA J. KOBAYASHI, *Gradient sensing limit of a cell when controlling the elongating direction*, 2024.
 - [38] CE. PLUNKETT AND SD. LAWLEY, *Boundary homogenization for patchy surfaces trapping patchy particles*, J. Chem. Phys., 158 (2023), p. 094104.
 - [39] S. REDNER, *A guide to first-passage processes*, Cambridge University Press, Cambridge, UK, 2001.
 - [40] TL. STEPIEN, C. ZMURCHOK, JB. HENGENIUS, RM. CAJA RIVERA, MR. D’ORSOGNA, AND AE. LINDSAY, *Moth mating: Modeling female pheromone calling and male navigational strategies to optimize reproductive success*, Appl. Sci., 10 (2020), p. 6543.
 - [41] MICHEAL J. WARD AND JOSEPH B. KELLER, *Strong localized perturbations of eigenvalue problems*, SIAM Journal on Applied Mathematics, 53 (1993), pp. 770–798.
 - [42] STEFANIE E. WINDNER, ANGELIKA MANHART, AMELIA BROWN, ALEX MOGILNER, AND MARY K. BAYLIES, *Nuclear scaling is coordinated among individual nuclei in multinucleated muscle fibers*, Developmental Cell, 49 (2019), pp. 48–62.e3.